

Review

2D-Nanolayer (2D-NL)-Based Hybrid Materials: A Next-Generation Material for Dye-Sensitized Solar Cells

Mohammad Ashfaq ^{1,*}, Neetu Talreja ^{2,*}, Neha Singh ³ and Divya Chauhan ^{4,*}

¹ Department of Biotechnology & University Centre for Research & Development (UCRD), Chandigarh University, Gharraun, Mohali 140413, Punjab, India

² Faculty of Science and Technology, Department of Science, Alliance University, Bengaluru 562106, Karnataka, India

³ Centre for Environmental Science and Engineering, Indian Institute of Technology Kanpur, Kanpur 208016, Uttar Pradesh, India

⁴ Department of Drinking Water and Sanitation, Ministry of Jal Shakti, 1208-A, Pandit Deendayal Antyodaya Bhawan, CGO Complex, Lodhi Road, New Delhi 110003, Delhi, India

* Correspondence: mohdashfaqbiotech@gmail.com (M.A.); neetutalreja99@gmail.com (N.T.); deep2424@gmail.com (D.C.)

Abstract: Two-dimensional (2D) materials, an electrifying family of innovative materials, have recently attracted wide attention due to their remarkable characteristics, primarily their high optical transparency, exceptional metallic conductivity, high mechanical strength, carrier mobility, tunable band gap values, and optimum work function. Interestingly, 2D-nanosheets/nanolayers (2D-NLs) might be synthesized into single/multi-layers using simple processes such as chemical vapor deposition (CVD), chemical bath deposition (CBD), and mechanical and liquid-phase exfoliation processes that simply enhance optoelectronic properties. However, the stability of 2D-NLs is one of the most significant challenges that limits their commercialization. Researchers have been focusing on the stability of 2D-NLs with the aim of developing next-generation solar cells. Easily tunable distinctive 2D-NLs that are based on the synthesis process, surface functional groups, and modification with other materials/hybrid materials thereby improve the stability of the 2D-NLs and their applicability to the hole transport layer (HTL) and the electron transport layer (ETL) in solar cells. Moreover, metal/non-metal-based dopants significantly enhance band gap ability and subsequently improve the efficacy of dye-sensitized solar cells (DSSCs). In this context, research has focused on 2D-NL-based photoanodes and working electrodes that improve the photoconversion efficiency (PCE) and stability of DSSCs. Herein, we mainly focus on synthesizing 2D-NLs, challenges during synthesis, stability, and high-performing DSSCs.

Keywords: two-dimensional materials; nanosheets; solar cells; optoelectronic devices; energy harvesting



Citation: Ashfaq, M.; Talreja, N.; Singh, N.; Chauhan, D. 2D-Nanolayer (2D-NL)-Based Hybrid Materials: A Next-Generation Material for Dye-Sensitized Solar Cells. *Electronics* **2023**, *12*, 570. <https://doi.org/10.3390/electronics12030570>

Academic Editors: Antonio Di Bartolomeo and Jr-Hau He

Received: 7 December 2022

Revised: 10 January 2023

Accepted: 21 January 2023

Published: 23 January 2023



Copyright: © 2023 by the authors. Licensee MDPI, Basel, Switzerland. This article is an open access article distributed under the terms and conditions of the Creative Commons Attribution (CC BY) license (<https://creativecommons.org/licenses/by/4.0/>).

1. Introduction

Presently, energy demand has been increasing with the growing population; globally, that inevitably decreases the amount of fossil fuels (oil, coal, and gases) and affects the environment. It is estimated that around 15 terawatts (TW) is consumed every year, which will increase to 30 TW by 2050. Approximately 80% of daily energy requirements are fulfilled by fossil fuels, whereas ~20% are fulfilled by renewable energy sources. The unremitting decrease in fossil fuels alongside increased energy consumption and environmental pollution as they burn increases the cost of raw materials/manufacturing. Usually, fossil fuel use, or the burning of fossil fuels, is a contributing factor to the production of greenhouse gases and, subsequently, global warming. Moreover, these fossil fuels are inadequate for the long term in terms of consumption rate [1–4]. Therefore, there is a need for renewable sources of energy that fulfil the energy demand without affecting the environment.

Researchers have continuously focused on fulfilling energy requirements by using renewable energy resources, especially sunlight, to produce electricity without impacting the environment. Solar power is an eco-friendly, simple, cost-effective route that converts photon energy into electricity. However, low solar conversion efficiency, non-ecofriendly materials/devices, complex fabrication processes, and the photovoltaic device's stability remain a concern [5–8]. In this aspect, researchers have continued to devote their efforts toward the design of semiconductor materials/photovoltaic devices with higher solar conversion efficiency, a simple fabrication process, and cost-effectiveness to resolve issues related to energy industries.

Several materials have been used so far for solar cell applications, including both metals (Zn, Fe, Ni, Ce, Cu, Cd, Pb, and TiO₂) and non-metals (fullerenes, carbon nanotubes (CNTs), carbon nanofibers (CNFs), graphene, graphene oxide (GO), and graphite). However, the relatively low conversion efficiency, toxicity, and stability of these metal/nonmetal-based solar cells is ongoing challenges nowadays [9–14]. Therefore, the requirement for newer materials/modifying existing semiconductor materials is to improve conversion efficiency, reduce toxicity, and enhance the stability of solar cells. In this aspect, two-dimensional nanolayers (2D-NLs) can improve solar conversion efficiency with high stability.

Recently, 2D-NLs have aroused widespread interest in their potential application in batteries, supercapacitors, environmental remediation, photocatalytic solar cells, antibiotic materials, wound dressing materials, and sensors. The 2D-NLs are in demand because of their incomparable characteristics, such as their charge carrying ability, tunable band gaps, high mechanical strength, high surface-to-volume ratios, and exceptional conductivity. Several 2D-NLs have been discovered (e.g., graphene, GO, TMDs (WS₂, MoS₂, TeS₂, etc.), black phosphorous, blue phosphorous, C₃N₄, MXene, boron nitride, and borophene) and effectively applied in numerous applications, such as agriculture, photocatalysis, the development of antibiotic materials, and the production of solar cells, mainly due to their nano-size thickness [15–28]. However, maintaining efficiency with such nano-metric thicknesses is one of the major concerns when fabricating solar cells. The thickness of 2D-NLs in a photovoltaic device is related to the stability of solar cells and can be controlled by changing their synthesis processes through methods such as liquid-phase exfoliation, chemical vapor deposition (CVD), chemical bath deposition (CBD), and hydrothermal synthesis, etc. Moreover, some methods are specific to synthesized single-layered structures with a thickness of 1 to 10 nm. CVD is one of the most popular methods for controlling thickness. The synthesized 2D-NLs can be used to design high-performance photovoltaic devices/solar cells.

Numerous types of solar cells/devices can be designed using 2D-NLs (either electron-transport layers (ETLs) or hole-transport layers (HTLs)), such as dye-sensitized solar cells (DSSCs), organic–inorganic solar cells, and perovskite solar cells (PSCs), etc. However, achieving high photo conversion efficiency (PCE) and stability is still a concern, as the stability of 2D-NLs is one of the greatest challenges when designing solar cells. Therefore, research is still required to enhance the stability of 2D-NLs for solar cell application. In this aspect, several methods have been adopted to alter the electronic structure of 2D-NLs, including metal or non-metal doping and surface functionalization using organic and inorganic moieties. Tuning the electronic properties might impact the band gap structure, and lowering the conduction band up to the desired value directly impacts the efficiency of solar cells as photoelectrons might be easily captured by photoactive material and thus take part in the final reaction. Another important property that needs to be considered is the solar cell's flexibility. Polymeric, paper, and fabric-based substrates have recently been used to achieve portability and flexibility in 2D-NLs. As these substrates can perform a dual role, (1) these substrates can provide mechanical strength to the 2D-NLs and (2) they can help enhance their surface area. This review focuses mainly on the current status of solar cells, different 2D-NL-based DSSCs, and their conversion efficiency. We also discuss the stability and performance prospects of the 2D-NL–hybrid material-based DSSCs, such as how to improve the stability of the 2D-NL hybrid materials used in high-performance

DSSCs. This review might provide newer insight into the generation of next-generation solar cell devices.

2. Solar Cells and Their Current Status

The incessant growth of the market for solar cells/panels since 1980 is due to their ability to operate as multi-megawatt power plants. The current scenario of the solar cells/panels market is growth of around 30–40%; this became possible mainly due to reduced costs, better reliability, and the economic development of solar cell supply. DSSCs are feasible and appropriate replacements for conventional energy sources such as solar power. They have emerged as one of the substitutes for extensively used silicon-based photovoltaic devices that convert solar energy to electrical energy.

In contrast, modern solar cells are primarily based on the creation of electron holes composed mainly of two layers (p- and n-type semiconductor materials). Usually, in solar irradiation imposed on the p- and n-type materials, it is the electron that has been ejected that moves from one layer to another layer. It creates an electron and a hole, thus producing energy [6,8,29–31]. Solar cells can be categorized based on semiconductor materials, including the following: (1) Crystalline silicon (c-Si) solar cells. c-Si solar cells utilize crystalline silicon and mainly single or multi-crystalline junction types. They are normally brittle and rigid. However, they still preferred due to their cost effectiveness. (2) Thin film-based solar cells. These second-generation solar cells are fabricated using thin films to decrease the cost of manufacture, with the trade-off being lower effectiveness compared to single crystal cells (except expensive gallium arsenide (GaAs) cells). (3) Hybrid solar cells. The third-generation of solar cell technologies which mainly consists of multi-junction cells, organic photovoltaic (OPV) cells, and hybrid solar cells. Hybrid solar cells employ inorganic and organic semiconductor material combinations, which can be seen DSSCs and perovskite solar cells. Moreover, hybrid solar cells are yet to make a noteworthy entry into large-scale commercial applications [32–38]. Usually, materials with high power generation efficiency enable the development of smaller and more cost-effective solar cells. The highest PCE, ~25.6%, was achieved for single junction-based solar cells (monocrystalline solar cells). Moreover, monocrystalline solar cells are one of the pillars of the market. However, high production cost, a sophisticated fabrication process, and energy payback time (EPBT) remain a concern. In this aspect, researchers have focused on decreasing production costs, simplifying the fabrication process, and tuning EPBT. With the help of relatively inexpensive vapor deposition processes/equipment, researchers have successfully reduced the cost of solar cells and simplified fabrication by reducing the utilization of semiconductor materials. Vapor deposition techniques contribute considerably to the simplified fabrication of thin film-based solar cells. The highest associated PCE of ~21.5% was achieved with CdTe-solar cells, which was lower than single junction-based solar cells [39,40]. In recent years, organic and hybrid material-based solar cells have shown great potential in terms of accomplishing solar conversion efficiency and stability improvements, especially for flexible solar cell devices.

3. 2D-NL-Based Solar Active Materials

2D-NL-based materials (graphene, graphene oxide, WS_2 , MOS_2 , MXene, TiO_2 , and ZnO) are a newer class of materials with different characteristics, such as surface phenomena and interface chemistry with their bulk materials. Furthermore, symmetrical lowering at the interface prevents newer environments from being manageable in the bulk equivalent. Consequently, the physicochemical characteristics, such as photon involvement in redox reactions, an acid base, and catalytic reactivity, are different and maybe dissuade the design of newer materials. Therefore, 2D-NLs are considered revolutionary due to their potential to fulfil the demand for next-generation solar cells with high power conversion efficiency (PCE). In this aspect, researchers have continued to focus on developing 2D-NL-based solar cells. Usually, incorporating 2D-NLs within the solar cells might enhance charge transport and the absorption of light while suppressing the carrier recombination that

leads to an enhancement in PCE with the increased fill factor (FF) and short-circuit current density (J_{sc}) of OSCs. Moreover, appropriate 2D-NLs might be replaced with an unstable layer of solar cells, which is one of the possible strategies for improving next-generation highly stable solar cells. With this approach, the PCE of DSSCs, organic solar cells, and organic perovskite solar cells significantly improved by more than ~12%, 18%, and 25%, respectively [41–46]. Researchers are currently focusing on newer semiconductor materials, the combination of two or three materials, or hybrid material-based solar cells that might improve PCE and stability.

4. Strategies to Improve Stability

Global energy demand and rapid population growth necessitate the high performance and stability of next-generation DSSCs. The high PCE and stability of DSSCs supports their increased share in the market. However, the stability and PCE of the DSSCs remains a concern for commercialization. Moreover, long-term uses in real-time operation remain a concern for commercialization. Numerous strategies have been applied to augment the stability and PCE of DSSCs, such as the incorporation of metals, the use of polymers or carbon, surface functionalization, the design of heterojunctions, the application of 2D-NLs, and control of the thickness of 2D-NLs. Incorporating these materials might improve dye adsorption ability and mesoporosity, help tune the band gap, and increase conductivity, thereby improving the PCE and stability of DSSCs [47–51].

Usually, a dopant is an impurity that is incorporated into a bulk matrix to tune/adjust semiconductor properties. With the help of dopant materials, structural and electronic properties can be easily tuned, which might be advantageous for crystallinity, band gap value, and the relocation of electrons to the conduction band. Usually, two types of dopant materials can tune the band gap value: (1) organic dopants and (2) inorganic dopants. Organic dopants such as metals can change the electronic structure of the materials and subsequently, their band gap value. Band gap tuning facilitates the movement of electrons to the next energy level so that photon energy can be easily captured. The captivated energy helps the electron eject from the valence band. Numerous studies have suggested that the metals and their oxides that efficiently decrease/increase band gap values subsequently improve the performance of the semiconductor materials [52–57]. Inorganic dopants are a class of dopants that includes carbon-based nanomaterials (CB-NMs) such as carbon nanotubes (CNTs), carbon nanofibers (CNFs), graphene, GO, and rGO. CB-NMs exhibit high tensile strength, a large surface area, and large pore size distribution and can therefore be effectively used in numerous applications, including DSSCs. Interestingly, carbon-based 2D-NLs such as graphene, GO, and rGO have gained considerable attention, particularly in terms of application in electronics and solar cells. This is largely due to their unique characteristics, such as high surface area, high conductivity, and flexibility. The conductivity of the graphene, GO, and rGO mainly depends on the number of layers that directly affect electronic properties, thus affecting the PCE of solar cells [58–64].

Usually, 2D-NL-based doping within the other 2D-NL materials attracts interest due to their excellent electronic, optical, and mechanical characteristics. The single/multi-layer of these dopant (2D-NLs) materials provides exceptional surface area, large pore volume, and beneficial charge transport ability, making them a favorable candidate for solar cell application as an absorbing layer, HTL, or ETL with the aim of amplifying the performance and stability of solar cells, including DSSCs. Moreover, achieving high PCE and stability with DSSCs is one of the greatest challenges for commercialization. With the incorporation of 2D-NLs, we can easily enhance the PCE and stability of the solar cells, including DSSCs. It is important to mention here that excess incorporation of dopants might decrease PCE; therefore, the optimum amount of dopants should be determined for high PCE-based DSSCs.

5. 2D-NL-Based DSSCs

DSSCs, a type of third-generation solar cell, have advanced significantly since their invention in 1991 by Brian O'Regan and Michael Grätzel. Numerous advantages make these cells exceptional solar devices, mainly recyclability, environmental friendliness, chemical stability, high energy conversion efficiency, and high artificial light performance. Moreover, roll-to-roll production and high energy efficiency are not the only advantages of using DSSCs. Since their productivity does not decline with increasing temperatures, this extends the efficiency of harvesting energy from sunlight [65–70]. DSSCs have five essential components: (1) transparent conducting oxide (TCO), i.e., glass substrate, (2) a photoanode (a coating of direct bandgap semiconductor materials on TCO), (3) a photosensitizer, (4) a cathode (carbon–platinum layer on TCO), and (5) an electrolyte [71–73]. When solar irradiation strikes the photoanode surface, the adsorbed dye molecules are photo-stimulated, producing excited electrons. The excited electrons move through the TCO and jump into the conduction band, producing an electric current. It is important to mention that degradation of DSSC preformation is one of the greatest challenges nowadays at multiple levels, including the molecular, module or panel, cell, and system levels. Usually, a DSSC's complex system, either the photoanode, dye, or electrolyte on their own, does not generate electricity, but when these elements come together with an accurate balance in all aspects (mainly diffusion that effectively controls the components of solar cells) they produce solar cells with high stability [74–77]. Figure 1 shows a schematic illustration of the different components of DSSCs. In general, the PCE and stability of the DSSCs depends on each component; therefore, it is necessary to improve each component to enhance the PCE and stability of these cells. In this regard, researchers have continued looking towards newer materials with high stability and PCE for the production of next-generation solar cells.

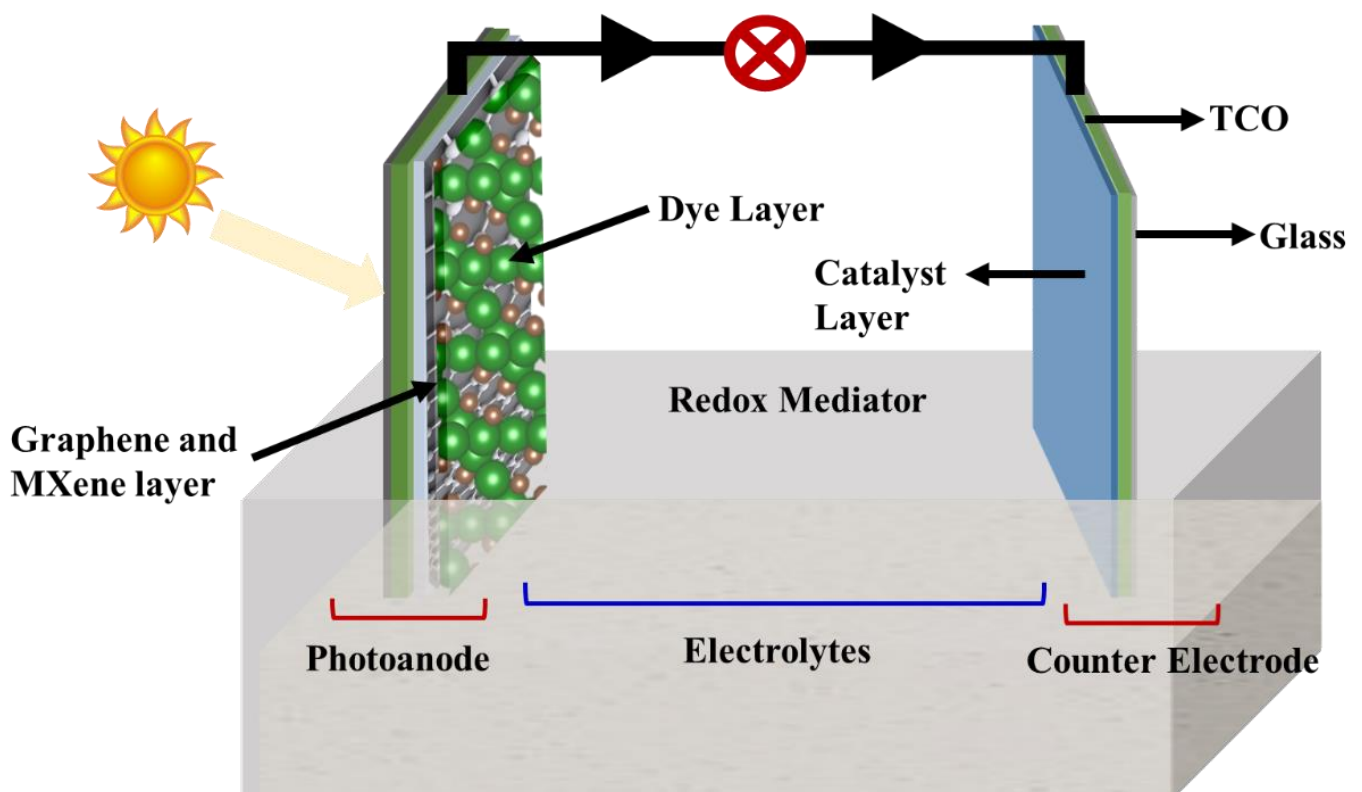


Figure 1. Schematic illustration of the different components of DSSCs.

5.1. Graphene and Its Derivative-Based DSSCs

Graphene, the first synthesized 2D-NL, has gained a remarkable amount of attention from researchers due to its unique characteristics, mainly its exceptional carrier mobility. Another class of graphene-like oxygen-containing derivatives of graphene or graphene oxide (GO) and reduced graphene oxide (rGO) has also been comprehensively applied in numerous applications (including environmental remediation, photocatalysis, energy, the dressing of materials, and solar cells) because of their high carrier mobility, great conductivity, high dispersion ability, and high biocompatibility [78–80]. Numerous methods and precursors have been used to synthesize graphene in order to increase the PCE of solar cells. Organic and inorganic functional groups have been incorporated within the graphene skeleton through simple covalent interaction between the GO and other functional groups, thus providing stability and PCE. Incorporating these functional moieties facilitated unceasing diffusion paths between the donor and acceptor interfaces that led to the conquest/suppression of exciton recombination and the promotion of charge transport. Graphene can be decorated with metal nanoparticles that tune intrinsic properties for photovoltaic applications. Moreover, a derivative of graphene (rGO) has good conductivity compared to GO. Furthermore, stacking interaction and poor dispersion ability make individual rGO sheets inaccessible in terms of modification or functionalization. However, research into preventing aggregation and achieving high PCE with rGO and other graphene-based composites continues. Several studies have reported about the application of graphene and graphene-based derivatives in high-performance DSSCs. For instance, Ju et al. synthesized N-doped graphene (N-graphene) using a two-step reaction sequence, which was further deposited over fluorine-doped SnO₂ (FTO)/glass substrates using an electro spray technique. The synthesized N-graphene showed a PCE of 9.05% with a fill factor of 74.2% [81]. Using hydrothermal synthesis, Yu et al. synthesized dual atom (nitrogen and sulfur)-doped graphene (N-S-graphene). Nitrogen and sulfur co-doped graphene was used as a metal-free counter electrode (CE) in DSSCs. Due to the synergistic effect of dual atoms in graphene, it shows high catalytic activity towards I₃[−] reduction. The large surface area and interconnectivity of pores facilitate mass transfer, which exhibits a PCE of 9.40% [82]. Paranthaman et al. synthesized rGO through the thermal reduction of GO and applied it as a CE in DSSCs. The surface area and pore size distribution of synthesized rGO were 110.16 m² g^{−1} and 0.5182 cm³ g^{−1}, respectively, thus supporting electrolyte migration and a higher PCE of 5.8% [83]. Casaluci et al. synthesized graphene using a liquid-phase exfoliation process and applied it as a CE for DSSCs. The data suggested that graphene-based CEs could be used effectively in DSSCs (PCE of 3.5%) [84]. Zhang et al. synthesized graphene using an exfoliation process and dispersed it onto FTO glass. The prepared graphene-based CE was annealed to create a 3D structure that improved PCE (6.81%) [85]. Prasad et al. synthesized rGO-Cu₂S-based composite materials and deposited them on onto FTO glass using an electrochemical method to fabricate quantum dot-based DSSCs. Figure 2 includes SEM images of the Cu₂S and rGO-Cu₂S at lower and higher magnification levels. The images indicate the uniform wrapping of rGO within the Cu₂S. The synthesized rGO-Cu₂S nanocomposites demonstrated a PCE of 4.26% using organic electrolytes, with short-circuit current density (J_{sc}), open circuit voltage (V_{oc}), and fill factor of 17.2 mA cm^{−2}, 0.57 V, and 44%, respectively [86].

Jiang et al. synthesized Co₃S₄-NS-rGO-based composites using a hydrothermal process and applied them as CEs for DSSCs. The synthesized Co₃S₄-NS-rGO-based nanocomposite showed a PCE of 8.08%. Interestingly, Co₃S₄-NS shows excellent reduction skills for I₃[−] compared to the bulk and more active sites for the catalytic reaction [87]. Ngidi et al. synthesized dual atom (pyridinic and pyrrolic N)-doped rGO (N-N-rGO) using the hydrothermal method. Synthesized dual atom-doped rGO exhibited a large surface area of 161.51 m² g^{−1} and enhanced electrical conductivity of 22.07 S cm^{−1}. The presence of dual atoms enhanced iodide reduction and subsequently led to higher PCE (4.13%) compared to pristine rGO [88]. Salleh et al. synthesized nickel sulfide-doped rGO (Ni-S-rGO) to fabricate DSSCs. The prepared Ni-S-rGO-based DSSCs showed PCE of 1.42% due to the

incorporation of thiourea that improved the reduction current [89]. Khoa et al. thermally synthesized rGO and synthesized a platinum (rGO-Pt)-based nanocomposite using a spray technique to apply them as CEs in DSSCs. The data suggested that rGO-Pt improved electron transport in the photoanode, thereby leading to high PCE (5.78%). The hybrid rGO-Pt composite reduced recombination by providing electrons to the I^-/I_3^- electrolyte, which significantly increased the PCE of DSSCs [90]. Khan et al. synthesized polypyrrole-graphene (P-graphene)-based Pt-free DSSCs. The data suggested that the P-graphene could be used effectively in DSSCs with PCE of 3.06% with 4% graphene content within the composite [91]. Oh et al. synthesized graphene-Cu₂ZnNiSe₄-WO₃ (GCZNSW) using a hydrothermal process and applied it as a CE for DSSCs. The data indicate that the prepared GCZNSW-based hybrid composite achieved 12.16% PCE, which is greater than the Pt electrode and suggests that the prepared GCZNSW-based hybrid composite has the potential ability to replace it [92]. The aforementioned studies and Table 1 (a summary of graphene and composite DSSCs) suggests that graphene and graphene composite materials can be used efficiently as photoanode and CE materials in DSSCs due to superior performance stemming from their exceptional surface area, wide-range absorption spectrum, high conductivity, improved photon absorption, and excellent electron transport. The doping of metals/polymers within the graphene significantly affects the PCE of the DSSCs. Moreover, the environmental friendliness and high stability of graphene and its composite materials make them promising candidates for future DSSCs.

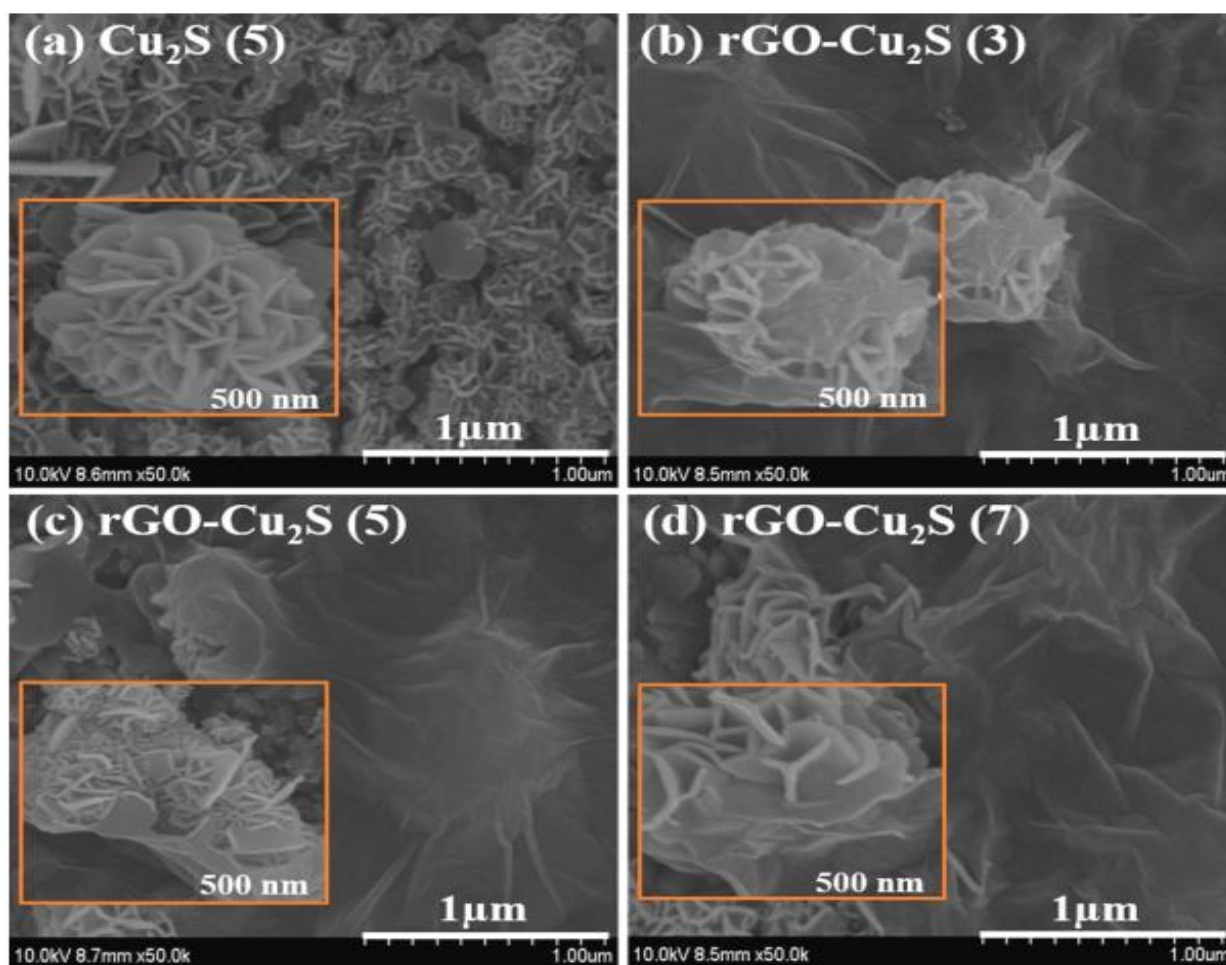


Figure 2. SEM images of (a) Cu₂S and (b–d) rGO-Cu₂S. The images have been reproduced with permission [86].

Table 1. Graphene and graphene composite-based DSSCs.

S. No.	Graphene and Graphene Composites	Synthesis Process	PCE (%)	Remarks	References
1.	N-graphene	E-spray deposition	9.05	A thin film of N-graphene-based CEs shows high PCE.	[81]
2.	N-S-graphene	Hummer's method	9.40	The dual atom (N-S) doping of graphene improved PCE.	[82]
3.	rGO	Thermal process	5.8	rGO facilitates electrolyte migration and, subsequently, higher PCE.	[83]
4.	Graphene	Liquid-phase exfoliation	3.5	Large surface area and high transparency might replace Pt.	[84]
5.	Graphene	Liquid-phase exfoliation	6.81	Graphene-based CE annealing creates a 3D network that improves PCE.	[85]
6.	rGO-Cu ₂ S	Electrochemical deposition	4.26	The uniform wrapping of rGO within Cu ₂ S improved PCE.	[86]
7.	Co ₃ S ₄ -NS-rGO	Hydrothermal	8.08	Co ₃ S ₄ -NS improved reduction ability for I ₃ ⁻ more than bulk and created more active sites for catalytic reaction, thereby leading to higher PCE.	[87]
8.	N-N-rGO	Hydrothermal	4.13	The dual atom-doped rGO improved the tri-iodic reduction reaction, thereby leading to higher PCE.	[88]
9.	Ni-S-rGO	Hummer's method and spin coating	1.42	The sulfur content improved PCE while also exhibiting a high reduction current.	[89]
10.	rGO-Pt	Hummer's method and a thermal process	5.78	rGO-Pt improved electron transport in the photoanode.	[90]
11.	P-graphene	Polymerization	3.06	Graphene content affected PCE.	[91]
12.	GCZNSW	Hydrothermal	12.16	The graphene-based hybrid electrode showed higher PCE than Pt.	[92]

5.2. TiO₂-Based DSSCs

TiO₂ is the most chosen semiconductor material due to its inexpensive cost, high adsorption ability, and non-toxicity. Moreover, TiO₂ is a frequently utilized semiconductor due to its excellent dispersion and degree of crystallinity. The 2D-NLs, especially those with mesoporous structure, play a crucial role in DSSCs because of their high surface area, larger pore volume, and tunable nanostructure, which results in high adsorption ability toward dye molecules and a high ability to receive electrons from an excited dye. The dye injects an electron into the conduction band of the 2D-NLs during photoexcitation, which is then followed by transmission to the reference/CE (counter) that completes the cycle. Several studies have suggested the effective use of TiO₂ in DSSCs. For example, Yu et al. synthesized TiO₂ nanosheets (TiO₂-NS) using a hydrothermal process and HF acid was used as a shape-controlling agent for the fabrication of DSSCs. Figure 3 shows the SEM, TEM, and HR-TEM images of TiO₂-NS that confirm the formation of 2D-NL-based TiO₂. The high crystallinity, pore volume, and exceptional light scattering ability of TiO₂-NS enable higher PCE (4.56%) compared to other types of TiO₂, such as TiO₂ nanoparticles (4.24%) and commercial grade T25 TiO₂ nanoparticles (3.64%). The data suggest that 2D-NLs might improve the PCE of DSSCs [93]. Wu et al. synthesized TiO₂-NS using a simple hydrothermal process and fabricated DSSCs where TiO₂-NS was used as a scattering layer. TiO₂-NS improves PCE (7.54%) compared to the use of TiO₂ nanoparticles. Exceptional light scattering offers rapid charge transfer, the least resistance, and high charge collection [94]. Peng et al. synthesized TiO₂-NS with a highly exposed facet (001) using a hydrothermal process and fabricated DSSCs. TiO₂-NS achieved PCE of 8.77%, which was higher than commercial grade T25 TiO₂ nanoparticles (6.92%) due to higher photocurrent density [95]. Laskova et al. synthesized crystal faces of (001) and (101) with TiO₂-NS and tested them against DSSCs. The data indicate that the different crystal face of TiO₂-NS shows different PCE, and the highest PCE (4.7%) was ultimately observed with TiO₂-NS (101) [96].

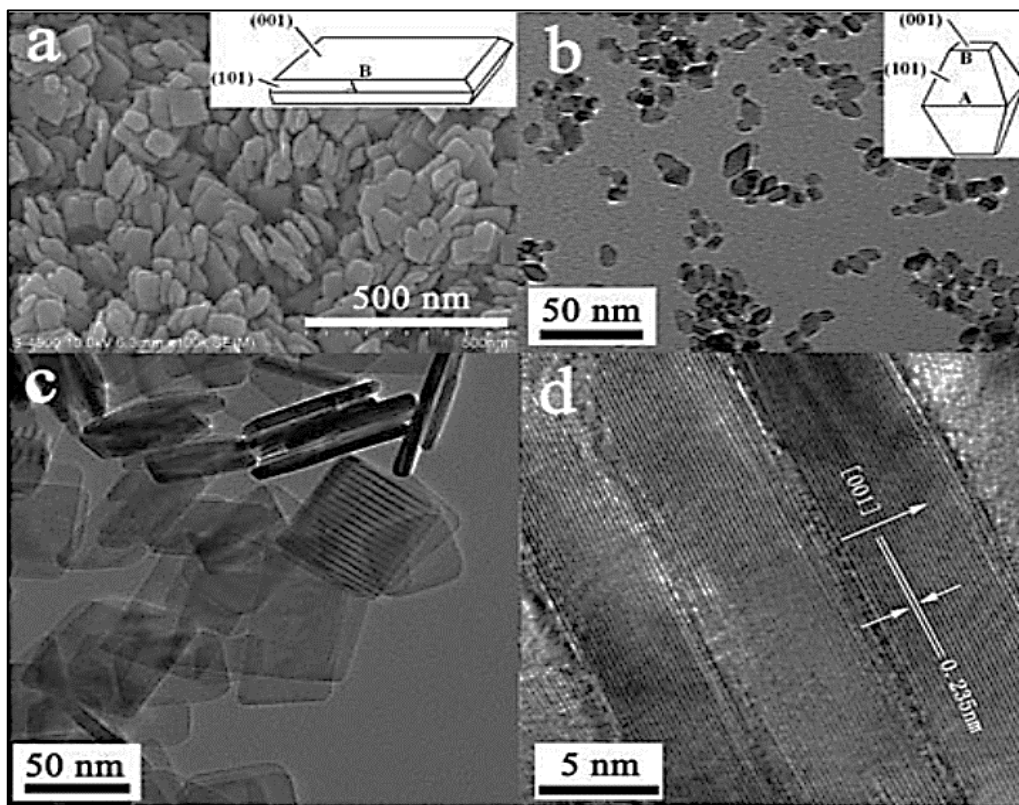


Figure 3. (a) SEM, (b,c) TEM, and (d) HR-TEM images of TiO_2 -NS. The images have been reproduced with permission [93].

Numerous modifications have been made to semiconductors with the aim of improving the photovoltaic effects of DSSCs, including the doping of transition metals and polymers. For example, Miles et al. synthesized TiO_2 -NS onto ZnO nanowires (TiO_2 -NS-ZNW) and fabricated DSSCs. Figure 4 shows the SEM and TEM images of ZnO nanowires and TiO_2 -NS-ZNW. The images show a uniform coating of TiO_2 -NS on the ZnO nanowires. The prepared TiO_2 -NS-ZNW-based DSSCs show 7.5% PCE, which is around 30% more than that of TiO_2 . The significant improvement in PCE is mainly due to the improved surface area, electron transport, and light scattering ability. Moreover, bare ZnO nanowire-based DSSCs decrease PCE and stability, whereas the smaller quantity of TiO_2 -NS drastically improves the performance of DSSCs [97]. Jiang et al. synthesized Niobium-doped TiO_2 -NS (Nb- TiO_2 -NS) and used it as a photoelectrode for DSSCs. The theoretical study suggested that Nb- TiO_2 -NS might achieve 10% PCE, which is around 22% higher than without the use of doped TiO_2 -based DSSCs [98]. Xu et al. synthesized g- C_3N_4 -incorporated TiO_2 -NS using a simple heating process and applied it in DSSCs. The data suggested that g- C_3N_4 - TiO_2 -NS is effectively used in DSSCs with a PCE of 7.34%, largely due to the additional electron in the photoanode. Moreover, incorporating urea and g- C_3N_4 within g- C_3N_4 - TiO_2 -NS increases PCE [99]. Lin et al. synthesized ZnO-NS using the chemical bath deposition (CBD) technique and incorporated it with TiO_2 (ZnO-NS/ TiO_2). The data indicate that the ZnO-NS-based DSSCs show PCE of 6.6%, whereas incorporating TiO_2 significantly improved PCE to 7.07%, which was attributed to TiO_2 increasing dye loading ability [100]. Kim et al. synthesized ZnO-NS using an electrochemical process and incorporated it with CdSe and TiO_2 to produce CdSe-ZnO-NS and TiO_2 -ZnO-NS and applied it for the fabrication of DSSCs. The data suggested that, upon the incorporation of CdSe and TiO_2 within ZnO-NS, PCE increased compared to the use of bare ZnO-NS. Moreover, CdSe-ZnO-NS-based DSSCs show the highest PCE (1.30%), whereas TiO_2 -ZnO-NS shows PCE of around 0.70%. The improvement in PCE is due to the inhibited recombination of electron hole pairs at the interface of CdSe and TiO_2 [101]. The aforementioned studies and Table 2

suggest that TiO₂-NS is the most commonly used 2D-NL in DSSCs due to its high adsorption ability, cost-effectiveness, mesoporous texture, ability to receive electrons from dye, and high crystallinity. Moreover, TiO₂-NS shows higher PCE than other forms of TiO₂, such as nanoparticles and commercially available TiO₂, because the 2D-NL form of TiO₂ increases surface area and thereby leads to higher adsorption ability toward dye molecules. Interestingly, the doping of transition metals and polymers within TiO₂-NS considerably improved the PCE of DSSCs. Therefore, TiO₂-NS-based hybrid materials might become next-generation materials for DSSCs with high PCE and stability.

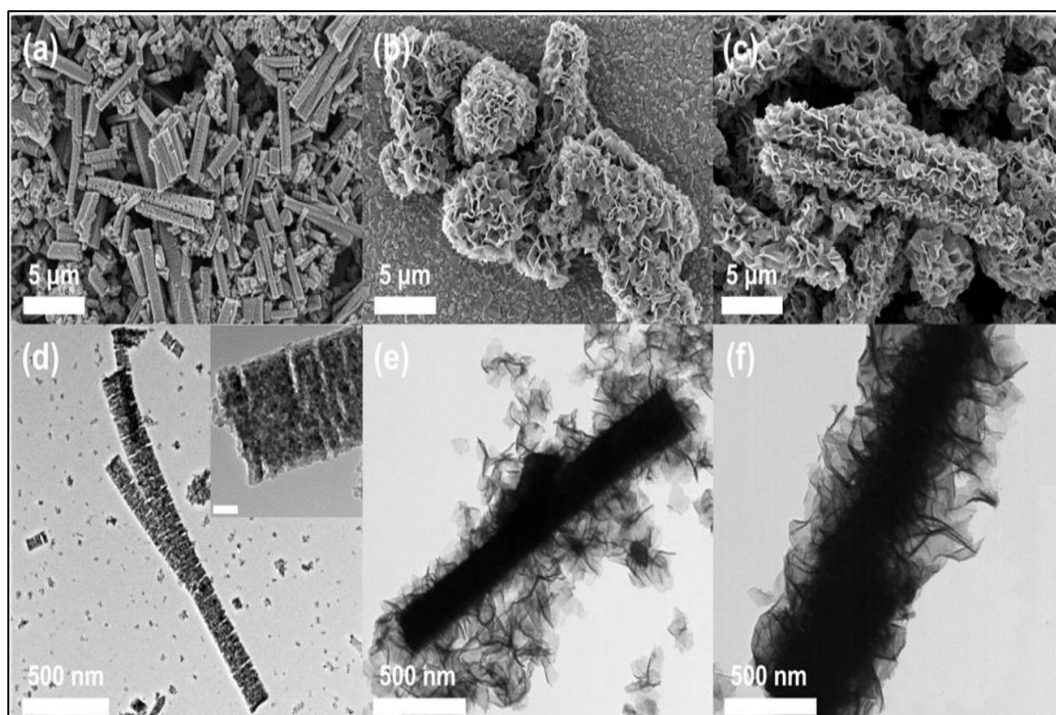


Figure 4. SEM images of (a) ZnO nanowires and (b,c) TiO₂-NS-ZNW and TEM images of (d) ZnO nanowires and (e,f) TiO₂-NS-ZNW. The images have been reproduced with permission [97].

Table 2. TiO₂-NS and TiO₂-NS composite materials for DSSCs.

S. No.	TiO ₂ -NS and TiO ₂ -NS Composites	Synthesis Process	PCE (%)	Remarks	References
1.	TiO ₂ -NS	Hydrothermal	4.56	TiO ₂ -NS shows high PCE compared to TiO ₂ nanoparticles.	[93]
2.	TiO ₂ -NS	Hydrothermal	7.54	TiO ₂ -NS improves charge transfer and has the least resistance.	[94]
3.	TiO ₂ -NS	Hydrothermal	8.77	TiO ₂ -NS shows higher photocurrent density than TiO ₂ nanoparticles.	[95]
4.	TiO ₂ -NS	Hydrothermal	4.7	Different crystal faces of TiO ₂ -NS show different PCE.	[96]
5.	TiO ₂ -NS-ZNW	Hydrothermal	7.5	The incorporation of TiO ₂ -NS significantly improved the performance of solar cells.	[97]
6.	Nb-TiO ₂ -NS	–	10	Incorporation of Nb within Nb-TiO ₂ -NS significantly improves PCE.	[98]
7.	g-C ₃ N ₄ -TiO ₂ -NS	Heating process	7.34	The incorporation of g-C ₃ N ₄ within TiO ₂ -NS significantly improves PCE.	[99]
8.	ZnO-NS/TiO ₂	CBD	7.07	The incorporation of TiO ₂ within ZnO-NS significantly improved dye loading and PCE.	[100]
9.	CdSe-ZnO-NS and TiO ₂ -ZnO-NS	Electrochemical deposition	1.30 and 0.70	The incorporation of CdSe and TiO ₂ within ZnO-NS significantly improved PCE.	[101]

5.3. MXene-Based DSSCs

MXenes are a newer class of transition metal carbides and/or nitrides that were discovered by Gogotsi and W. Barsoum in 2011. MXene, a newer class of ceramic material, has been attracting attention due to its high conductivity (10^5 S cm^{-1}) that stems from high mechanical strength and flexibility. This high conductivity is applied in the hole transport layer, electron transport layer, and protective layer of advanced solar cells. However, synthesis complications limit their application. In particular, acid-based exfoliation requires modification in terms of synthesis, as green synthesis is preferred over the use of acids. The excessive use of strong acid (especially HF acid) for the exfoliation of MXene layers from the MAX phase requires further consideration in terms of large-scale applications. However, high tensile strength, high conductivity, and a tunable band gap prove applicability to photovoltaics.

MXene-based materials have very low band gaps, which promote recombination. The higher the recombination rate, the lower the electric properties of the NLs. To use these materials for solar cell devices, there must be a minimal band gap so that the flow of electrons from the valence band to the conduction band can be maintained. Doping and functionalization can tune the band gap of MXene-based materials [102–104]. MXene has gained continuous interest and is extensively used in numerous applications, including environmental remediation, photocatalysis, energy storage, solar cell, biocidal agent, and biomedical applications [20,105–109]. Recently, a few studies have suggested that MXene and its hybrid materials can be used effectively for the development of high-performance DSSCs. For example, Dall’Agnese et al. synthesized MXene and TiO_2 (MXene- TiO_2)-based photoanodes and oxidized them at a different temperature to improve the performance of DSSCs. The data suggested that upon increasing the oxidizing temperature, PCE continuously increased up to $450 \text{ }^\circ\text{C}$ (2.66%). However, a temperature of more than $450 \text{ }^\circ\text{C}$ decreased the DSSC performance, mainly due to the smaller surface area [110]. Chen et al. synthesized MXene-CoS using an etching process and a hydrothermal process. Initially, MXene was synthesized by a simple etching process that involved HF acid. Next, the heterostructure composite was synthesized using a hydrothermal process. Figure 5 shows the SEM and TEM images and elemental mapping of MXene and the MXene-CoS-based composite. The SEM images indicate that the separated MXene sheets and CoS nanoparticles attached to MXene sheets. Moreover, no changes in the layer were observed after incorporating the CoS nanoparticles into the MXene, which makes it a suitable candidate for DSSCs. The data suggest that the prepared MXene-CoS-based composite shows high electrochemical performance (8.09% PCE). The high PCE of the MXene-CoS-based composite, mainly due to MXene-NS and the incorporation of CoS nanoparticles, creates more catalytic sites that improve permeability and charge transfer; therefore, MXene might become a next-generation material that could be used in the production of solar cells [111].

Another study focused on the use of Poly (3,4-ethylene dioxythiophene) (PEDOT)-decorated MXene (PEDOT-MXene) in DSSCs. Figure 6 shows a schematic representation of the PEDOT-MXene. The PEDOT-MXene-based DSSCs showed high electrochemical activity and mass transport ability, with PCE of 7.12%. Moreover, the prepared PEDOT-MXene-based DSSCs were stable for up to 15 days and an increase in PCE of around 40% was observed, which suggests that PEDOT-MXene-based DSSCs having the potential ability to replace Pt-based DSSCs [112]. Wen et al. synthesized a MXene-reduced graphene oxide (rGO)-polyethylene oxide/poly(vinylidene fluoride-co-hexafluoropropylene) (MXene-rGO-P)-based composite for use as a printable electrolyte. The data suggested that rGO and polymer incorporation within the MXene improves PCE. The maximum PCE observed was 8.255% [113]. Ahmad et al. synthesized MXene to replace the Pt and transparent conducting oxide (TCO) layer used in DSSCs. The data suggested that TCO- and Pt-free MXene were effective when used in DSSCs, as shown by 8.68% PCE. Moreover, PCE mainly depends on the thickness of MXene. PCE increased with the increasing thickness of MXene (up to $8 \text{ }\mu\text{m}$ thickness) [114]. The literature suggests that MXene can potentially be applied to the development of solar cells, especially DSSCs with high PCE, thus replacing TCO

and Pt within DSSCs. Moreover, incorporating other 2D-NLs, polymers, and nanoparticles within the MXene significantly improved PCE due to enhanced surface area, conductivity, adsorption of dye/loading of dye, and permeability. Moreover, the thickness of the MXene layer is an important factor that directly affects the PCE of DSSCs.

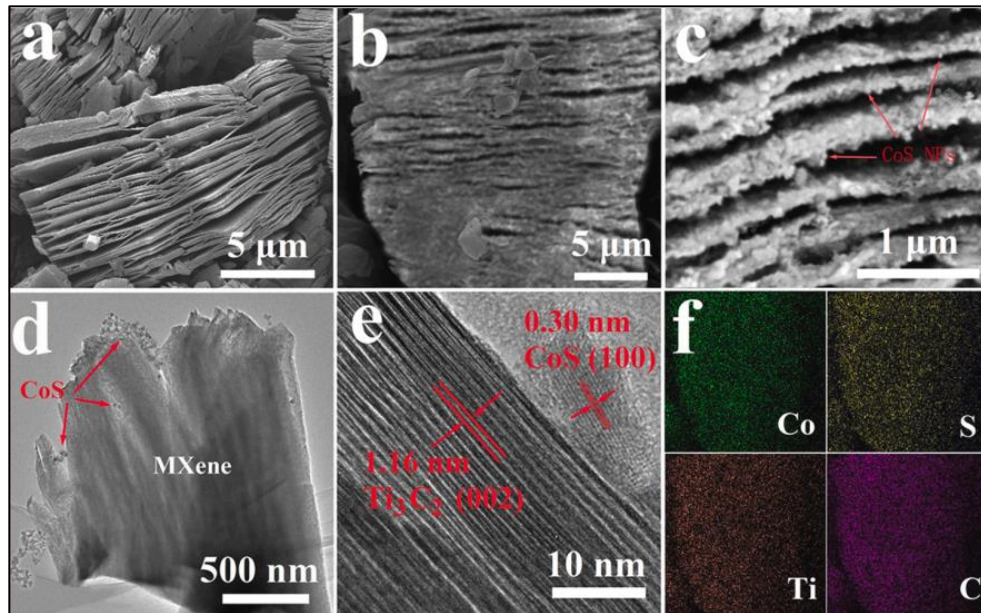


Figure 5. SEM images of (a) MXene and (b,c) MXene-CoS, TEM images of (d,e) MXene-CoS, and (f) an elemental mapping of MXene-CoS. The images have been reproduced with permission [111].

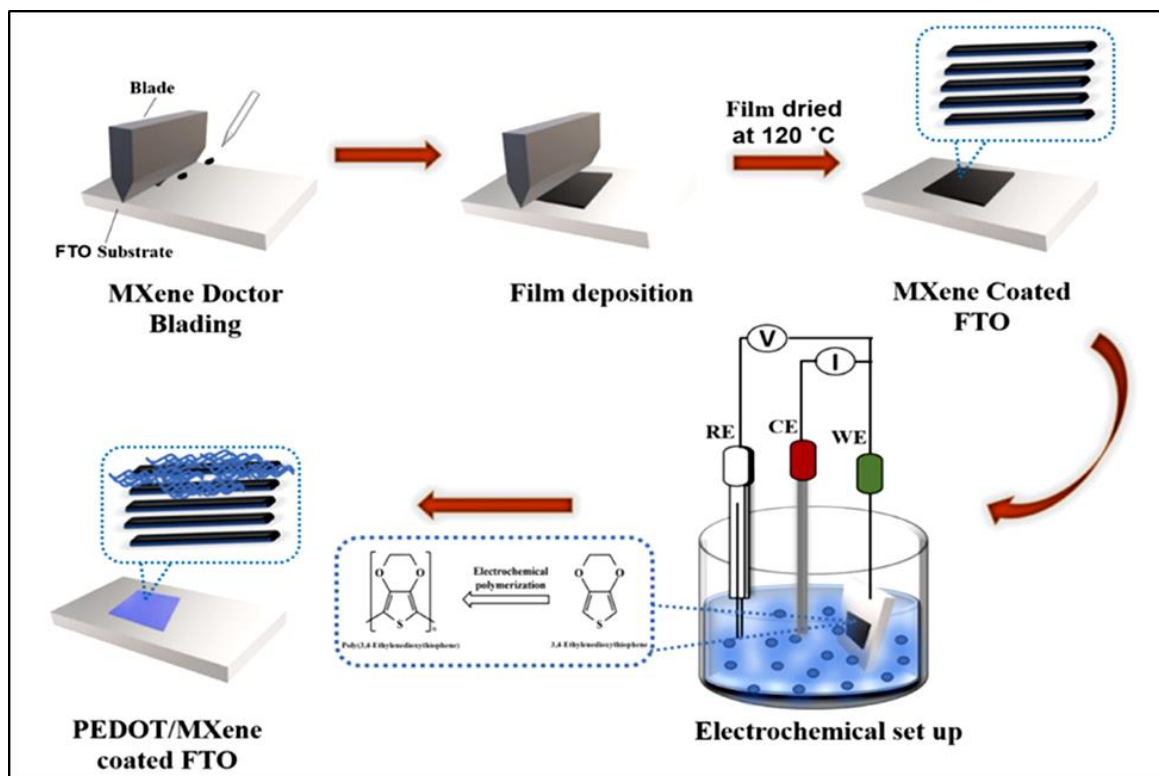


Figure 6. A schematic illustration of a PEDOT-MXene-based DSSC. The images have been reproduced with permission [112].

5.4. Black Phosphorus (BP)-Based DSSCs

BP is a novel class of 2D-NL that is highly reactive under normal conditions and therefore unstable. BP was synthesized using a liquid-phase exfoliation process and demonstrated exceptional performance, mainly in terms of energy, biomedical, electronic, sensor, and solar cell applications. The high applicability of BP is mainly due to the tunable band gap value and high carrier mobility, which makes BP a promising candidate for solar cell applications. However, poor stability and high-density charge transfer limit the applicability of BP in solar cells [115–119]. So far, few studies have been conducted concerning the fabrication of high-performance solar cells, especially DSSCs with high stability. For instance, Xu et al. synthesized a BP-TiO₂-based photoanode that was used in DSSCs. The prepared BP-TiO₂-based DSSCs showed 9.73% PCE, which is higher than TiO₂-based DSSCs (6.98%). Moreover, the high PCE of the BP-TiO₂-based DSSCs is due to charge separation and transfer [120]. Song et al. synthesized BP-TiO₂-based electrodes for the fabrication of DSSCs. The photon adsorption ability of BP-TiO₂ depends on the number of layers. The BP-TiO₂-based DSSCs showed high PCE that represented an improvement of ~38% compared to TiO₂ [121]. For future research, surface-modified BP incorporating metals, polymers, and other 2D-NLs might provide better PCE and easily replace Pt electrodes.

5.5. Other 2D-NL-Based DSSCs

Another interesting group of 2D-NLs that has been efficiently used for solar cell applications is TMDs (MoS₂, MoSe₂, WS₂, WSe₂, TiS₂, TiSe₂, TeS₂, VSe₂, NbSe₂, etc.). Usually, TMDs are mainly composed of MX₂ (M (transition metal) and X (chalcogen)), where M is a sandwich between two X layers using covalent bonds and Vander Waal forces. MoS₂- and WS₂-NLs have been effectively used in various types of applications (including the areas of antibiotic materials, energy, the environment, and solar cells) due to their extraordinary characteristics, such as high surface area, transparency, high conductivity, a tunable band gap, and high biocompatibility [22,122–125]. The tunable band gap's ability to change its thickness is one of the fascinating characteristics of TMDs that might be beneficial for solar cell applications [126]. Numerous TMD-based 2D-NLs have been effectively used to fabricate solar cells such as DSSCs. For instance, Gurulakshmi et al. synthesized MoS₂-based CEs for DSSCs using an electrodeposition process. The data suggested that the MoS₂-based CEs were effective when used in DSSCs, as shown by 4.21% PCE [127]. Vijaya et al. synthesized MoS₂ and graphene-MoS₂ using a hydrothermal process and fabricated CEs for DSSCs. The data suggested that graphene-MoS₂ shows higher PCE (8.1%) than MoS₂ (6.6%) [128]. Krishnamoorthy et al. synthesized MoS₂ and a graphene-MoS₂-based photoanode for DSSCs. Interestingly, the incorporation of graphene within MoS₂ reduced the band gap value and reduced the recombination of electron photogeneration, thus subsequently improving PCE to 8.92%, which is higher than bare MoS₂ (3.36% PCE) [129]. Menon et al. synthesized TiO₂-incorporated MoS₂ (TiO₂-MoS₂)-based photoanodes for DSSCs. The data indicate that the TiO₂-MoS₂-based DSSCs show a high PCE of 6.0% compared to the bare TiO₂-based DSSCs (4.7% PCE), mainly due to high photoadsorption. Moreover, more than 0.1% MoS₂ decreases the PCE of the DSSCs [130]. Xu et al. synthesized PEDOT-MoS₂-based CEs for DSSCs. The data suggested that incorporating MoS₂ within PEDOT effectively improved PCE to 7.0% [131]. Li et al. synthesized WS₂-based CEs for DSSCs using the doctor blade method. Incorporation of TiO₂ and carbon particles within the WS₂ film improved conductivity and adhesion, thus significantly improving the PCE of the DSSCs. The fabricated DSSCs with the prepared TiO₂/carbon particles/WS₂-based counter showed 4.56% PCE [132]. Krishnamoorthy et al. synthesized graphene-incorporated WS₂ (graphene-WS₂)-based photoanodes for the fabrication of DSSCs. Incorporating graphene within WS₂ improved the adsorption ability of the dye, which significantly improved PCE. The prepared graphene-WS₂-based DSSCs showed 9.6% PCE. The high PCE is mainly due to the large surface area and mesoporous property of graphene-WS₂-based photoanodes [133]. Huang et al. synthesized CoS₂-N-C-Co-WS₂-based CEs for the fabrication of DSSCs. The prepared CoS₂-N-C-Co-

WS₂-based composite had a large surface area and yolk–shell structure that improved PCE. The prepared CoS₂-N-C-Co-WS₂-based DSSCs showed a high PCE of 9.21%, which is comparatively higher than Pt [134]. Hussain et al. synthesized CuS-WS₂- and CuS-MoS₂-based CEs to fabricate DSSCs. The sulfur-based heterostructure improved electrocatalytic activity and decreased charge transfer resistance, thus improving PCE. The prepared CuS-WS₂- and CuS-MoS₂-based DSSCs showed 8.21% and 7.12% PCE, which is comparable to Pt-based electrodes [135]. The aforementioned studies and Table 3 summarize the different 2D-NLs, including TMDs that are effectively used as photoanodes and CEs in the fabrication of DSSCs. Moreover, incorporating metal, carbon, and polymers significantly improved the PCE of DSSCs. Additionally, TMDs, mainly WS₂ and MoS₂, showed high or comparable PCE compared to the Pt-based DSSCs, suggesting that expensive Pt can be easily replaced with TMDs.

Table 3. Different 2D-NLs, their hybrid material-based DSSCs, and PCE.

S. No.	2D-NLs	Synthesis Process	PCE (%)	Remarks	References
1.	MXene-TiO ₂	Deposition	2.66	Increasing the oxidizing temperature improved PCE.	[110]
2.	MXene-CoS	Etching and hydrothermal	8.09	The incorporation of CoS nanoparticles within MXene improves permeability and PCE.	[111]
3.	PEDOT-MXene	Deposition	7.12	Incorporation of PEDOT within MXene improves PCE.	[112]
4.	MXene-rGO-P	Printing	8.255	The incorporation of rGO and co-polymer improves PCE.	[113]
5.	MXene	Etching	8.68	TCO- and Pt-free DSSCs show high PCE.	[114]
6.	MoS ₂	Electrodeposition	4.21	Surface modification of the electrode improves current density and PCE.	[127]
7.	MoS ₂ and graphene-MoS ₂	Hydrothermal	6.6 and 8.1	Graphene-incorporated MoS ₂ shows high PCE.	[128]
8.	Graphene-MoS ₂	Hydrothermal	8.92	Incorporation of graphene effectively reduces the band gap value and lowers photoelectron recombination.	[129]
9.	TiO ₂ -MoS ₂	Deposition	6.0	The incorporation of MoS ₂ within TiO ₂ increases PCE.	[130]
10.	PEDOT-MoS ₂	Hydrothermal	7.0	Incorporation of MoS ₂ within PEDOT significantly improves PCE.	[131]
11.	TiO ₂ /carbon particles/WS ₂	Deposition	4.56	TiO ₂ and carbon particles incorporated within WS ₂ improve the film's bonding and conductivity.	[132]
12.	Graphene-WS ₂	Hydrothermal	9.6	The incorporation of graphene within WS ₂ improves adsorption ability, thereby leading to higher PCE.	[133]
13.	CoS ₂ -N-C-Co-WS ₂	Sol–gel	9.21	The yolk–shell structure and high surface area improve PCE.	[134]
14.	CuS-WS ₂ and CuS-MoS ₂	CVD	8.21 and 7.12	High electrocatalytic activity and low charge transfer resistance improve PCE.	[135]

6. Conclusions

Researchers have continued to focus on the fabrication of DSSCs with different 2D-NLs (photoanode and CE) with the aim of enhancing the performance and stability of DSSCs in order to achieve higher or comparable PCE compared to commercially available solar cells. Moreover, researchers are also looking towards replacing the Pt-based electrode to reduce the cost of solar cells. Researchers and scientists in the solar cell industry are unremittingly working to develop a newer class of materials, including 2D-NL-based photoanodes and CEs that can considerably improve the PCE and stability of DSSCs. This review article focused on how 2D-NLs and their hybrid materials have been used as photoanode and CE materials in the fabrication of DSSCs. Previous studies have clearly shown that 2D-NLs significantly improve crystallinity, surface area, tuned band gap values, the adsorption of dye molecules, the migration of electrons, mass transfer, mesoporous properties, conductivity, flexibility, and electron transport while also facilitating light scattering, thereby improving the PCE of DSSCs. Moreover, incorporating dopants (metal, polymers, carbon particles, and other 2D-NLs) improved the PCE and stability of the DSSCs. It is important to mention here that the commercialization of DSSCs requires a simple process, cost-effectiveness, high PCE, and longer stability. With the help of 2D-NLs and their hybrid materials, we can easily resolve such issues and fulfil the requirements associated with the commercialization of DSSCs. Graphene-, MXene-, MoS₂-, and WS₂-based 2D-NLs have more active sites that facilitate the adsorption of dye molecules, thereby easily achieving high PCE and stability while also demonstrating the potential to replace Pt-based electrode materials in DSSCs. Moreover, further research on developing newer 2D-NLs and hybrid materials is still required to improve the PCE and stability of DSSCs.

Author Contributions: M.A., N.T. and D.C., conceptualized, writing, figures, and revised the manuscript. N.S. writing the manuscript. All authors have read and agreed to the published version of the manuscript.

Funding: This research received no external funding.

Conflicts of Interest: The authors declare no conflict of interest.

References

1. Kannan, N.; Vakeesan, D. Solar energy for future world: A review. *Renew. Sustain. Energy Rev.* **2016**, *62*, 1092–1105. [[CrossRef](#)]
2. Mekhilef, S.; Saidur, R.; Safari, A. A review on solar energy use in industries. *Renew. Sustain. Energy Rev.* **2011**, *15*, 1777–1790. [[CrossRef](#)]
3. Shafiee, S.; Topal, E. When will fossil fuel reserves be diminished? *Energy Policy* **2009**, *37*, 181–189. [[CrossRef](#)]
4. Asafu-Adjaye, J. The relationship between energy consumption, energy prices and economic growth: Time series evidence from Asian developing countries. *Energy Econ.* **2000**, *22*, 615–625. [[CrossRef](#)]
5. Kumar, J.C.R.; Majid, M.A. Renewable energy for sustainable development in India: Current status, future prospects, challenges, employment, and investment opportunities. *Energy Sustain. Soc.* **2020**, *10*, 2. [[CrossRef](#)]
6. Nayak, P.K.; Mahesh, S.; Snaith, H.J.; Cahen, D. Photovoltaic solar cell technologies: Analysing the state of the art. *Nat. Rev. Mater.* **2019**, *4*, 269–285. [[CrossRef](#)]
7. Kirchartz, T.; Rau, U. What Makes a Good Solar Cell? *Adv. Energy Mater.* **2018**, *8*, 1703385. [[CrossRef](#)]
8. Rathore, N.; Panwar, N.L.; Yettou, F.; Gama, A. A comprehensive review of different types of solar photovoltaic cells and their applications. *Int. J. Ambient Energy* **2021**, *42*, 1200–1217. [[CrossRef](#)]
9. Zhu, H.; Wei, J.; Wang, K.; Wu, D. Applications of carbon materials in photovoltaic solar cells. *Sol. Energy Mater. Sol. Cells* **2009**, *93*, 1461–1470. [[CrossRef](#)]
10. Deshmukh, M.A.; Park, S.-J.; Hedau, B.S.; Ha, T.-J. Recent progress in solar cells based on carbon nanomaterials. *Sol. Energy* **2021**, *220*, 953–990. [[CrossRef](#)]
11. Fei Guo, C.; Sun, T.; Cao, F.; Liu, Q.; Ren, Z. Metallic nanostructures for light trapping in energy-harvesting devices. *Light: Sci. Appl.* **2014**, *3*, e161. [[CrossRef](#)]
12. Sebastián, D.; Baglio, V.; Girolamo, M.; Moliner, R.; Lázaro, M.J.; Aricò, A.S. Carbon nanofiber-based counter electrodes for low cost dye-sensitized solar cells. *J. Power Sources* **2014**, *250*, 242–249. [[CrossRef](#)]
13. Batmunkh, M.; Biggs, M.J.; Shapter, J.G. Carbon Nanotubes for Dye-Sensitized Solar Cells. *Small* **2015**, *11*, 2963–2989. [[CrossRef](#)] [[PubMed](#)]
14. Muchuweni, E.; Martincigh, B.S.; Nyamori, V.O. Recent advances in graphene-based materials for dye-sensitized solar cell fabrication. *RSC Adv.* **2020**, *10*, 44453–44469. [[CrossRef](#)]
15. Sun, Z.; Talreja, N.; Tao, H.; Texter, J.; Muhler, M.; Strunk, J.; Chen, J. Catalysis of Carbon Dioxide Photoreduction on Nanosheets: Fundamentals and Challenges. *Angew. Chem. Int. Ed.* **2018**, *57*, 7610–7627. [[CrossRef](#)] [[PubMed](#)]
16. Tao, H.; Gao, Y.; Talreja, N.; Guo, F.; Texter, J.; Yan, C.; Sun, Z. Two-dimensional nanosheets for electrocatalysis in energy generation and conversion. *J. Mater. Chem. A* **2017**, *5*, 7257–7284. [[CrossRef](#)]
17. Gasso, S.; Mahajan, A. MXene based 2D-2D heterostructures for Counter Electrode in third generation Dye Sensitized Solar Cells. *Chem. Phys. Lett.* **2022**, *808*, 140144. [[CrossRef](#)]
18. Hussain, S.; Shaikh, S.F.; Vikraman, D.; Mane, R.S.; Joo, O.-S.; Naushad, M.; Jung, J. Sputtering and sulfurization-combined synthesis of a transparent WS₂ counter electrode and its application to dye-sensitized solar cells. *RSC Adv.* **2015**, *5*, 103567–103572. [[CrossRef](#)]
19. Talreja, N.; Chauhan, D.; Mangalaraja, R.V. Two-dimensional nanolayers for wearable supercapacitors. In *Nanostructured Materials for Sustainable Energy and Environmental Remediation*; IOP Publishing: Bristol, UK, 2022; pp. 3-1–3-20.
20. Talreja, N.; Ashfaq, M.; Chauhan, D.; Mangalaraja, R.V. Cu-MXene: A potential biocide for the next-generation biomedical application. *Mater. Chem. Phys.* **2023**, *294*, 127029. [[CrossRef](#)]
21. Chauhan, D.; Ashfaq, M.; Mangalaraja, R.V.; Talreja, N. 2D-Nanosheets Based Hybrid Nanomaterials Interaction with Plants. In *Nanomaterial Interactions with Plant Cellular Mechanisms and Macromolecules and Agricultural Implications*; Al-Khayri, J.M., Alnaddaf, L.M., Jain, S.M., Eds.; Springer International Publishing: Cham, Switzerland, 2023; pp. 299–316.
22. Ashfaq, M.; Talreja, N.; Chauhan, D.; Viswanathan, M.R. Synthesis of Cu-doped 2D-WS₂ nanosheet-based nano-antibiotic materials for inhibiting E. Coli and S. aureus bacterial strains. *New J. Chem.* **2022**, *46*, 5581–5587. [[CrossRef](#)]
23. Tomy, M.; Ambika Rajappan, A.; Vm, V.; Thankappan Suryabai, X. Emergence of Novel 2D Materials for High-Performance Supercapacitor Electrode Applications: A Brief Review. *Energy Fuels* **2021**, *35*, 19881–19900. [[CrossRef](#)]
24. Qin, Z.; Chen, Y.; Zhu, K.; Zhao, Y. Two-Dimensional Materials for Perovskite Solar Cells with Enhanced Efficiency and Stability. *ACS Mater. Lett.* **2021**, *3*, 1402–1416. [[CrossRef](#)]
25. Lin, Q.-L.; Liang, H.; Zhou, C.-Q.; Qian, Z.-F.; Sun, Y.-L.; Wang, X.-Y.; Wang, R.-H. Defect-induced magnetism in χ 3 borophene. *Rare Met.* **2022**, *41*, 3486–3494. [[CrossRef](#)]
26. Lin, Q.-L.; Qian, Z.-F.; Dai, X.-Y.; Sun, Y.-L.; Wang, R.-H. Regulation of electronic structure of monolayer MoS₂ by pressure. *Rare Met.* **2022**, *41*, 1761–1770. [[CrossRef](#)]

27. Lin, Q.; Miao, L.; Qian, Z.; Sun, Y.; Wang, R. First-Principles Calculations on Magnetism Induced by Vacancies in β 12-Borophene Nanosheets: Implications for Property Modulation. *ACS Appl. Nano Mater.* **2022**, *5*, 113–119. [[CrossRef](#)]
28. Wang, R.; Dai, X.; Qian, Z.; Zhong, S.; Chen, S.; Fan, S.; Zhang, H.; Wu, F. Boosting Lithium Storage in Free-Standing Black Phosphorus Anode via Multifunction of Nanocellulose. *ACS Appl. Mater. Interfaces* **2020**, *12*, 31628–31636. [[CrossRef](#)]
29. Al-Ezzi, A.S.; Ansari, M.N.M. Photovoltaic Solar Cells: A Review. *Appl. Syst. Innov.* **2022**, *5*, 67. [[CrossRef](#)]
30. Dambhare, M.V.; Butey, B.; Moharil, S.V. Solar photovoltaic technology: A review of different types of solar cells and its future trends. *J. Phys. Conf. Ser.* **2021**, *1913*, 012053. [[CrossRef](#)]
31. Li, J.; Aierken, A.; Liu, Y.; Zhuang, Y.; Yang, X.; Mo, J.H.; Fan, R.K.; Chen, Q.Y.; Zhang, S.Y.; Huang, Y.M.; et al. A Brief Review of High Efficiency III-V Solar Cells for Space Application. *Front. Phys.* **2021**, *8*, 631925. [[CrossRef](#)]
32. Ushasree, P.M.; Bora, B. Chapter 1 Silicon Solar Cells. In *Solar Energy Capture Materials*; The Royal Society of Chemistry: London, UK, 2019; pp. 1–55.
33. Satharasinghe, A.; Hughes-Riley, T. A Review of Solar Energy Harvesting Electronic Textiles. *Sensors* **2020**, *20*, 5938. [[CrossRef](#)]
34. Katagiri, H.; Jimbo, K.; Maw, W.S.; Oishi, K.; Yamazaki, M.; Araki, H.; Takeuchi, A. Development of CZTS-based thin film solar cells. *Thin Solid Films* **2009**, *517*, 2455–2460. [[CrossRef](#)]
35. Asim, N.; Mohammad, M.; Badieli, M. Chapter 8—Novel Nanomaterials for Solar Cell Devices. In *Nanomaterials for Green Energy*; Bhanvase, B.A., Pawade, V.B., Dhoble, S.J., Sonawane, S.H., Ashokkumar, M., Eds.; Elsevier: Amsterdam, The Netherlands, 2018; pp. 227–277.
36. Müller-Buschbaum, P.; Thelakkat, M.; Fässler, T.F.; Stutzmann, M. Hybrid Photovoltaics—From Fundamentals towards Application. *Adv. Energy Mater.* **2017**, *7*, 1700248. [[CrossRef](#)]
37. Michaels, H.; Benesper, I.; Freitag, M. Challenges and prospects of ambient hybrid solar cell applications. *Chem. Sci.* **2021**, *12*, 5002–5015. [[CrossRef](#)] [[PubMed](#)]
38. Lu, Z.; Hou, G.; Zhu, Y.; Chen, J.; Xu, J.; Chen, K. High efficiency organic–Si hybrid solar cells with a one-dimensional CdS interlayer. *Nanoscale* **2021**, *13*, 4206–4212. [[CrossRef](#)] [[PubMed](#)]
39. Lin, S.; Peng, X. Current Status and Challenges of Solar Cells Based on Semiconductor Nanocrystals. *Energy Fuels* **2021**, *35*, 18928–18941. [[CrossRef](#)]
40. Kim, M.R.; Ma, D. Quantum-Dot-Based Solar Cells: Recent Advances, Strategies, and Challenges. *J. Phys. Chem. Lett.* **2015**, *6*, 85–99. [[CrossRef](#)]
41. Sengupta, D.; Das, P.; Mondal, B.; Mukherjee, K. Effects of doping, morphology and film-thickness of photo-anode materials for dye sensitized solar cell application—A review. *Renew. Sustain. Energy Rev.* **2016**, *60*, 356–376. [[CrossRef](#)]
42. Devadiga, D.; Selvakumar, M.; Shetty, P.; Santosh, M.S. Recent progress in dye sensitized solar cell materials and photo-supercapacitors: A review. *J. Power Sources* **2021**, *493*, 229698. [[CrossRef](#)]
43. Castillo-Robles, J.A.; Rocha-Rangel, E.; Ramírez-de-León, J.A.; Caballero-Rico, F.C.; Armendáriz-Mireles, E.N. Advances on Dye-Sensitized Solar Cells (DSSCs) Nanostructures and Natural Colorants: A Review. *J. Compos. Sci.* **2021**, *5*, 288. [[CrossRef](#)]
44. Bera, S.; Sengupta, D.; Roy, S.; Mukherjee, K. Research into dye-sensitized solar cells: A review highlighting progress in India. *J. Phys. Energy* **2021**, *3*, 032013. [[CrossRef](#)]
45. Lee, C.-P.; Li, C.-T.; Ho, K.-C. Use of organic materials in dye-sensitized solar cells. *Mater. Today* **2017**, *20*, 267–283. [[CrossRef](#)]
46. Tontapha, S.; Uppachai, P.; Amornkitbamrung, V. Fabrication of Functional Materials for Dye-sensitized Solar Cells. *Front. Energy Res.* **2021**, *9*, 641983. [[CrossRef](#)]
47. Zhou, Q.; Duan, J.; Duan, Y.; Tang, Q. Review on engineering two-dimensional nanomaterials for promoting efficiency and stability of perovskite solar cells. *J. Energy Chem.* **2022**, *68*, 154–175. [[CrossRef](#)]
48. Chiu, W.-H.; Lee, K.-M.; Suryanarayanan, V.; Hsu, J.-F.; Wu, M.-C. Controlled Photoanode Properties for Large-Area Efficient and Stable Dye-Sensitized Photovoltaic Modules. *Nanomaterials* **2021**, *11*, 2125. [[CrossRef](#)]
49. Cheng, C.-K.; Lin, C.-H.; Wu, H.-C.; Ma, C.-C.M.; Yeh, T.-K.; Chou, H.-Y.; Tsai, C.-H.; Hsieh, C.-K. The Two-Dimensional Nanocomposite of Molybdenum Disulfide and Nitrogen-Doped Graphene Oxide for Efficient Counter Electrode of Dye-Sensitized Solar Cells. *Nanoscale Res. Lett.* **2016**, *11*, 117. [[CrossRef](#)] [[PubMed](#)]
50. Hsieh, C.-T.; Yang, B.-H.; Lin, J.-Y. One- and two-dimensional carbon nanomaterials as counter electrodes for dye-sensitized solar cells. *Carbon* **2011**, *49*, 3092–3097. [[CrossRef](#)]
51. Ghartavol, H.M.; Mohammadi, M.R.; Afshar, A.; Li, Y. On the assessment of incorporation of CNT–TiO₂ core–shell structures into nanoparticle TiO₂ photoanodes in dye-sensitized solar cells. *Photochem. Photobiol. Sci.* **2019**, *18*, 1840–1850. [[CrossRef](#)]
52. Roy-Mayhew, J.D.; Aksay, I.A. Graphene Materials and Their Use in Dye-Sensitized Solar Cells. *Chem. Rev.* **2014**, *114*, 6323–6348. [[CrossRef](#)]
53. Kim, S.-B.; Park, J.-Y.; Kim, C.-S.; Okuyama, K.; Lee, S.-E.; Jang, H.-D.; Kim, T.-O. Effects of Graphene in Dye-Sensitized Solar Cells Based on Nitrogen-Doped TiO₂ Composite. *J. Phys. Chem. C* **2015**, *119*, 16552–16559. [[CrossRef](#)]
54. Kundu, A.; Shit, A.; Nandi, S. Carbon Dot Assisted Synthesis of Nanostructured Polyaniline for Dye Sensitized Solar Cells. *Energy Fuels* **2017**, *31*, 7364–7371. [[CrossRef](#)]
55. Talreja, N.; Ashfaq, M.; Chauhan, D.; Mera, A.C.; Rodríguez, C.A. Strategic Doping Approach of the Fe–BiOI Microstructure: An Improved Photodegradation Efficiency of Tetracycline. *ACS Omega* **2021**, *6*, 1575–1583. [[CrossRef](#)] [[PubMed](#)]
56. Ünlü, B.; Çakar, S.; Özacar, M. The effects of metal doped TiO₂ and dithizone-metal complexes on DSSCs performance. *Sol. Energy* **2018**, *166*, 441–449. [[CrossRef](#)]

57. Kausar, A.; Sattar, A.; Xu, C.; Zhang, S.; Kang, Z.; Zhang, Y. Advent of alkali metal doping: A roadmap for the evolution of perovskite solar cells. *Chem. Soc. Rev.* **2021**, *50*, 2696–2736. [[CrossRef](#)] [[PubMed](#)]
58. Subalakshmi, K.; Chung, W.; Lee, S. Synergistically improved photovoltaic performances of dye-sensitized solar cells with metal-free organic cosensitizer and hybrid rGO-TiO₂ photoanode. *Dye. Pigment.* **2023**, *209*, 110892. [[CrossRef](#)]
59. Wu, Q.; Chen, R.; Su, P.; Shi, D.; Zhang, Y.; Chen, K.; Li, H. Co₉S₈/NC@FeCoS₂/NC composites with hollow yolk shell structure as the counter electrode for Pt-free dye-sensitized solar cells. *Electrochim. Acta* **2023**, *438*, 141587. [[CrossRef](#)]
60. Van Cuong, L.; Lam Tuan Cuong, D.; Tran Trung Nghia, L.; Khac Hung, L.; Thai Hoang, N.; Tan Nhiem, L.; Trong Liem Chau, P.; Thanh Phong, M.; Huu Hieu, N. Effect of reducing agents on co-precipitation synthesis of titanium dioxide/reduced graphene oxide composite materials for upgrading the performance of dye-sensitized solar cells. *Chem. Eng. Sci.* **2022**, *264*, 118145. [[CrossRef](#)]
61. Gupta, R.; Kumar, R.; Sharma, A.; Verma, N. Novel Cu-carbon nanofiber composites for the counter electrodes of dye-sensitized solar cells. *Int. J. Energy Res.* **2015**, *39*, 668–680. [[CrossRef](#)]
62. Ashfaq, M.; Chauhan, D.; Mangalaraja, R.V. Micro-mesoporous carbon-based nanostructured materials for flexible supercapacitors. In *Nanostructured Materials for Sustainable Energy and Environmental Remediation*; IOP Publishing: Bristol, UK, 2022; pp. 4-1–4-19.
63. Miao, X.; Tongay, S.; Petterson, M.K.; Berke, K.; Rinzler, A.G.; Appleton, B.R.; Hebard, A.F. High Efficiency Graphene Solar Cells by Chemical Doping. *Nano Lett.* **2012**, *12*, 2745–2750. [[CrossRef](#)]
64. Kadam, K.D.; Rehman, M.A.; Kim, H.; Rehman, S.; Khan, M.A.; Patil, H.; Aziz, J.; Park, S.; Abdul Basit, M.; Khan, K.; et al. Enhanced and Passivated Co-doping Effect of Organic Molecule and Bromine on Graphene/HfO₂/Silicon Metal-Insulator-Semiconductor (MIS) Schottky Junction Solar Cells. *ACS Appl. Energy Mater.* **2022**, *5*, 10509–10517. [[CrossRef](#)]
65. Hagfeldt, A.; Boschloo, G.; Sun, L.; Kloo, L.; Pettersson, H. Dye-Sensitized Solar Cells. *Chem. Rev.* **2010**, *110*, 6595–6663. [[CrossRef](#)]
66. Lin, L.-Y.; Ho, K.-C. Dye-Sensitized Solar Cells. In *Encyclopedia of Modern Optics*, 2nd ed.; Guenther, B.D., Steel, D.G., Eds.; Elsevier: Oxford, UK, 2018; pp. 270–281.
67. Sharma, K.; Sharma, V.; Sharma, S.S. Dye-Sensitized Solar Cells: Fundamentals and Current Status. *Nanoscale Res. Lett.* **2018**, *13*, 381. [[CrossRef](#)]
68. Ito, S.; Murakami, T.N.; Comte, P.; Liska, P.; Grätzel, C.; Nazeeruddin, M.K.; Grätzel, M. Fabrication of thin film dye sensitized solar cells with solar to electric power conversion efficiency over 10%. *Thin Solid Films* **2008**, *516*, 4613–4619. [[CrossRef](#)]
69. James, E.M.; Barr, T.J.; Meyer, G.J. Evidence for an Electronic State at the Interface between the SnO₂ Core and the TiO₂ Shell in Mesoporous SnO₂/TiO₂ Thin Films. *ACS Appl. Energy Mater.* **2018**, *1*, 859–867. [[CrossRef](#)]
70. Mathew, S.; Yella, A.; Gao, P.; Humphry-Baker, R.; Curchod, B.F.E.; Ashari-Astani, N.; Tavernelli, I.; Rothlisberger, U.; Nazeeruddin, M.K.; Grätzel, M. Dye-sensitized solar cells with 13% efficiency achieved through the molecular engineering of porphyrin sensitizers. *Nat. Chem.* **2014**, *6*, 242–247. [[CrossRef](#)]
71. Deepak, T.G.; Anjusree, G.S.; Thomas, S.; Arun, T.A.; Nair, S.V.; Sreekumaran Nair, A. A review on materials for light scattering in dye-sensitized solar cells. *RSC Adv.* **2014**, *4*, 17615–17638. [[CrossRef](#)]
72. Chen, H.; Liu, T.; Wang, B.; Liu, Z.; Li, Y.; Zhao, Q.; Wang, N.; He, H.; Liu, H.; Guo, Z. Highly efficient charge collection in dye-sensitized solar cells based on nanocomposite photoanode filled with indium-tin oxide interlayer. *Adv. Compos. Hybrid Mater.* **2018**, *1*, 356–363. [[CrossRef](#)]
73. Snaith, H.J.; Schmidt-Mende, L. Advances in Liquid-Electrolyte and Solid-State Dye-Sensitized Solar Cells. *Adv. Mater.* **2007**, *19*, 3187–3200. [[CrossRef](#)]
74. Iftikhar, H.; Sonai, G.G.; Hashmi, S.G.; Nogueira, A.F.; Lund, P.D. Progress on Electrolytes Development in Dye-Sensitized Solar Cells. *Materials* **2019**, *12*, 1998. [[CrossRef](#)]
75. Cavallo, C.; Di Pascasio, F.; Latini, A.; Bonomo, M.; Dini, D. Nanostructured Semiconductor Materials for Dye-Sensitized Solar Cells. *J. Nanomater.* **2017**, *2017*, 5323164. [[CrossRef](#)]
76. Asim, N.; Ahmadi, S.; Alghoul, M.A.; Hammadi, F.Y.; Saeedfar, K.; Sopian, K. Research and Development Aspects on Chemical Preparation Techniques of Photoanodes for Dye Sensitized Solar Cells. *Int. J. Photoenergy* **2014**, *2014*, 518156. [[CrossRef](#)]
77. Kharkwal, D.; Sharma, N.; Kumar Gupta, S.; Mohan Singh Negi, C. Enhanced performance of dye-sensitized solar cells by co-sensitization of metal-complex and organic dye. *Sol. Energy* **2021**, *230*, 1133–1140. [[CrossRef](#)]
78. Sasidharan, V.; Sachan, D.; Chauhan, D.; Talreja, N.; Ashfaq, M. Three-dimensional (3D) polymer—Metal—carbon framework for efficient removal of chemical and biological contaminants. *Sci. Rep.* **2021**, *11*, 7708. [[CrossRef](#)]
79. Ashfaq, M.; Talreja, N.; Chauhan, D.; Rodríguez, C.A.; Mera, A.C.; Ramalinga Viswanathan, M. Synthesis of reduced graphene oxide incorporated bimetallic (Cu/Bi) nanorods based photocatalyst materials for the degradation of gallic acid and bacteria. *J. Ind. Eng. Chem.* **2022**, *110*, 447–455. [[CrossRef](#)]
80. Ashfaq, M.; Wongpakham, T.; Talreja, N.; Chauhan, D.; Tharasanit, T.; Srituravanich, W. Synthesis of polymeric composite grafted with mineral particles/graphene oxide-based biomaterial: A promising robust hemostatic bandage. *Mater. Today Commun.* **2022**, *33*, 104786. [[CrossRef](#)]
81. Ju, M.J.; Kim, J.C.; Choi, H.-J.; Choi, I.T.; Kim, S.G.; Lim, K.; Ko, J.; Lee, J.-J.; Jeon, I.-Y.; Baek, J.-B.; et al. N-Doped Graphene Nanoplatelets as Superior Metal-Free Counter Electrodes for Organic Dye-Sensitized Solar Cells. *ACS Nano* **2013**, *7*, 5243–5250. [[CrossRef](#)] [[PubMed](#)]
82. Yu, Z.; Bai, Y.; Wang, Y.; Liu, Y.; Zhao, Y.; Liu, Y.; Sun, K. One-step synthesis of three-dimensional nitrogen and sulfur co-doped graphene networks as low cost metal-free counter electrodes for dye-sensitized solar cells. *Chem. Eng. J.* **2017**, *311*, 302–309. [[CrossRef](#)]

83. Paranthaman, V.; Sundaramoorthy, K.; Chandra, B.; Muthu, S.P.; Alagarsamy, P.; Perumalsamy, R. Investigation on the Performance of Reduced Graphene Oxide as Counter Electrode in Dye Sensitized Solar Cell Applications. *physica status solidi a* **2018**, *215*, 1800298. [[CrossRef](#)]
84. Casaluci, S.; Gemmi, M.; Pellegrini, V.; Di Carlo, A.; Bonaccorso, F. Graphene-based large area dye-sensitized solar cell modules. *Nanoscale* **2016**, *8*, 5368–5378. [[CrossRef](#)]
85. Zhang, D.W.; Li, X.D.; Li, H.B.; Chen, S.; Sun, Z.; Yin, X.J.; Huang, S.M. Graphene-based counter electrode for dye-sensitized solar cells. *Carbon* **2011**, *49*, 5382–5388. [[CrossRef](#)]
86. Krishna Prasad, A.; Jo, I.-R.; Kang, S.-H.; Ahn, K.-S. Novel method for synthesis of reduced graphene oxide–Cu₂S and its application as a counter electrode in quantum-dot-sensitized solar cells. *Appl. Surf. Sci.* **2021**, *564*, 150393. [[CrossRef](#)]
87. Jiang, T.; Yang, S.; Dai, P.; Yu, X.; Bai, Z.; Wu, M.; Li, G.; Tu, C. Economic synthesis of Co₃S₄ ultrathin nanosheet/reduced graphene oxide composites and their application as an efficient counter electrode for dye-sensitized solar cells. *Electrochim. Acta* **2018**, *261*, 143–150. [[CrossRef](#)]
88. Ngidi, N.P.D.; Muchuveni, E.; Nyamori, V.O. Dual heteroatom-doped reduced graphene oxide and its application in dye-sensitized solar cells. *Opt. Mater.* **2021**, *122*, 111689. [[CrossRef](#)]
89. Salleh, S.A.; Rahman, M.Y.A.; Aziz, T.H.T. Dye-sensitized solar cell using nickel sulfide-reduced graphene oxide counter electrode: Effect of sulphur content. *Inorg. Chem. Commun.* **2022**, *135*, 109086. [[CrossRef](#)]
90. Khoa, N.T.; Thuan, D.V.; Kim, S.W.; Park, S.; Tam, T.V.; Choi, W.M.; Cho, S.; Kim, E.J.; Hahn, S.H. Facile fabrication of thermally reduced graphene oxide–platinum nanohybrids and their application in catalytic reduction and dye-sensitized solar cells. *RSC Adv.* **2016**, *6*, 1535–1541. [[CrossRef](#)]
91. Mahmood Khan, I.; Nazar, R.; Mehmood, U. Development of polypyrrole/graphene (PPY/graphene) based electrocatalyst for platinum free dye-sensitized solar cells (DSSCs). *Mater. Lett.* **2022**, *320*, 132331. [[CrossRef](#)]
92. Oh, W.C.; Cho, K.Y.; Jung, C.H.; Areerob, Y. Hybrid of Graphene based on quaternary Cu₂ZnNiSe₄–WO₃ Nanorods for Counter Electrode in Dye-sensitized Solar Cell Application. *Sci. Rep.* **2020**, *10*, 4738. [[CrossRef](#)]
93. Yu, J.; Fan, J.; Lv, K. Anatase TiO₂ nanosheets with exposed (001) facets: Improved photoelectric conversion efficiency in dye-sensitized solar cells. *Nanoscale* **2010**, *2*, 2144–2149. [[CrossRef](#)] [[PubMed](#)]
94. Wu, C.; Qi, L.; Chen, Y.; Ouyang, Q.; Li, C. Dye-sensitized solar cells based on two-dimensional TiO₂ nanosheets as the scattering layers. *Res. Chem. Intermed.* **2016**, *42*, 5653–5664. [[CrossRef](#)]
95. Peng, J.-D.; Shih, P.-C.; Lin, H.-H.; Tseng, C.-M.; Vittal, R.; Suryanarayanan, V.; Ho, K.-C. TiO₂ nanosheets with highly exposed (001)-facets for enhanced photovoltaic performance of dye-sensitized solar cells. *Nano Energy* **2014**, *10*, 212–221. [[CrossRef](#)]
96. Laskova, B.; Zukalova, M.; Kavan, L.; Chou, A.; Liska, P.; Wei, Z.; Bin, L.; Kubat, P.; Ghadiri, E.; Moser, J.E.; et al. Voltage enhancement in dye-sensitized solar cell using (001)-oriented anatase TiO₂ nanosheets. *J. Solid State Electrochem.* **2012**, *16*, 2993–3001. [[CrossRef](#)]
97. Miles, D.O.; Lee, C.S.; Cameron, P.J.; Mattia, D.; Kim, J.H. Hierarchical growth of TiO₂ nanosheets on anodic ZnO nanowires for high efficiency dye-sensitized solar cells. *J. Power Sources* **2016**, *325*, 365–374. [[CrossRef](#)]
98. Jiang, L.; Sun, L.; Yang, D.; Zhang, J.; Li, Y.-J.; Deng, W.-Q. Niobium-Doped (001)-Dominated Anatase TiO₂ Nanosheets as Photoelectrode for Efficient Dye-Sensitized Solar Cells. *ACS Appl. Mater. Interfaces* **2017**, *9*, 9576–9583. [[CrossRef](#)] [[PubMed](#)]
99. Xu, J.; Wang, G.; Fan, J.; Liu, B.; Cao, S.; Yu, J. g-C₃N₄ modified TiO₂ nanosheets with enhanced photoelectric conversion efficiency in dye-sensitized solar cells. *J. Power Sources* **2015**, *274*, 77–84. [[CrossRef](#)]
100. Lin, C.-Y.; Lai, Y.-H.; Chen, H.-W.; Chen, J.-G.; Kung, C.-W.; Vittal, R.; Ho, K.-C. Highly efficient dye-sensitized solar cell with a ZnO nanosheet-based photoanode. *Energy Environ. Sci.* **2011**, *4*, 3448–3455. [[CrossRef](#)]
101. Kim, Y.T.; Park, M.Y.; Choi, K.H.; Tai, W.S.; Shim, W.H.; Park, S.Y.; Kang, J.W.; Lee, K.H.; Jeong, Y.; Kim, Y.D.; et al. ZnO nanosheets decorated with CdSe and TiO₂ for the architecture of dye-sensitized solar cells. *J. Nanosci. Nanotechnol.* **2011**, *11*, 2263–2268. [[CrossRef](#)] [[PubMed](#)]
102. Saeed, M.A.; Shahzad, A.; Rasool, K.; Mateen, F.; Oh, J.-M.; Shim, J.W. 2D MXene: A Potential Candidate for Photovoltaic Cells? A Critical Review. *Adv. Sci.* **2022**, *9*, 2104743. [[CrossRef](#)] [[PubMed](#)]
103. Yin, L.; Li, Y.; Yao, X.; Wang, Y.; Jia, L.; Liu, Q.; Li, J.; Li, Y.; He, D. MXenes for Solar Cells. *Nano-Micro Lett.* **2021**, *13*, 78. [[CrossRef](#)]
104. Shi, Z.; Khaledialidusti, R.; Malaki, M.; Zhang, H. MXene-Based Materials for Solar Cell Applications. *Nanomaterials* **2021**, *11*, 3170. [[CrossRef](#)]
105. Wang, Y.; Guo, T.; Tian, Z.; Bibi, K.; Zhang, Y.-Z.; Alshareef, H.N. MXenes for Energy Harvesting. *Adv. Mater.* **2022**, *34*, 2108560. [[CrossRef](#)]
106. Sun, Y.; Li, Y. Potential environmental applications of MXenes: A critical review. *Chemosphere* **2021**, *271*, 129578. [[CrossRef](#)]
107. Agresti, A.; Pazniak, A.; Pescetelli, S.; Di Vito, A.; Rossi, D.; Pecchia, A.; Auf der Maur, M.; Liedl, A.; Larciprete, R.; Kuznetsov, D.V.; et al. Titanium-carbide MXenes for work function and interface engineering in perovskite solar cells. *Nat. Mater.* **2019**, *18*, 1228–1234. [[CrossRef](#)] [[PubMed](#)]
108. Li, X.; Bai, Y.; Shi, X.; Su, N.; Nie, G.; Zhang, R.; Nie, H.; Ye, L. Applications of MXene (Ti₃C₂T_x) in photocatalysis: A review. *Mater. Adv.* **2021**, *2*, 1570–1594. [[CrossRef](#)]
109. Ramezani Farani, M.; Nourmohammadi Khiarak, B.; Tao, R.; Wang, Z.; Ahmadi, S.; Hassanpour, M.; Rabiee, M.; Saeb, M.R.; Lima, E.C.; Rabiee, N. 2D MXene nanocomposites: Electrochemical and biomedical applications. *Environ. Sci. Nano* **2022**, *9*, 4038–4068. [[CrossRef](#)]

110. Dall'Agnese, C.; Dall'Agnese, Y.; Anasori, B.; Sugimoto, W.; Mori, S. Oxidized Ti₃C₂ MXene nanosheets for dye-sensitized solar cells. *New J. Chem.* **2018**, *42*, 16446–16450. [[CrossRef](#)]
111. Chen, X.; Zhuang, Y.; Shen, Q.; Cao, X.; Yang, W.; Yang, P. In situ synthesis of Ti₃C₂T_x MXene/CoS nanocomposite as high performance counter electrode materials for quantum dot-sensitized solar cells. *Sol. Energy* **2021**, *226*, 236–244. [[CrossRef](#)]
112. Priya Nagalingam, S.; Grace, A.N. Poly(3,4-ethylenedioxythiophene) decorated MXene as an alternative counter electrode for dye-sensitized solar cells. *Mater. Today Chem.* **2022**, *26*, 101113. [[CrossRef](#)]
113. Wen, J.; Sun, Z.; Qiao, Y.; Zhou, Y.; Liu, Y.; Zhang, Q.; Liu, Y.; Jiao, S. Ti₃C₂ MXene-Reduced Graphene Oxide Composite Polymer-Based Printable Electrolyte for Quasi-Solid-State Dye-Sensitized Solar Cells. *ACS Appl. Energy Mater.* **2022**, *5*, 3329–3338. [[CrossRef](#)]
114. Ahmad, M.S.; Pandey, A.K.; Abd Rahim, N.; Aslfattahi, N.; Mishra, Y.K.; Rashid, B.; Saidur, R. 2-D Mxene flakes as potential replacement for both TCO and Pt layers for Dye-Sensitized Solar cell. *Ceram. Int.* **2021**, *47*, 27942–27947. [[CrossRef](#)]
115. Yang, Y.; Gao, J.; Zhang, Z.; Xiao, S.; Xie, H.-H.; Sun, Z.-B.; Wang, J.-H.; Zhou, C.-H.; Wang, Y.-W.; Guo, X.-Y.; et al. Black Phosphorus Based Photocathodes in Wideband Bifacial Dye-Sensitized Solar Cells. *Adv. Mater.* **2016**, *28*, 8937–8944. [[CrossRef](#)]
116. Xue, Y.; Min, S.; Wang, F. Dye-sensitized black phosphorus nanosheets decorated with Pt cocatalyst for highly efficient photocatalytic hydrogen evolution under visible light. *Int. J. Hydrog. Energy* **2019**, *44*, 21873–21881. [[CrossRef](#)]
117. Lin, S.; Li, Y.; Qian, J.; Lau, S.P. Emerging opportunities for black phosphorus in energy applications. *Mater. Today Energy* **2019**, *12*, 1–25. [[CrossRef](#)]
118. Chen, W.; Ouyang, J.; Liu, H.; Chen, M.; Zeng, K.; Sheng, J.; Liu, Z.; Han, Y.; Wang, L.; Li, J.; et al. Black Phosphorus Nanosheet-Based Drug Delivery System for Synergistic Photodynamic/Photothermal/Chemotherapy of Cancer. *Adv. Mater.* **2017**, *29*, 1603864. [[CrossRef](#)] [[PubMed](#)]
119. Wang, X.; Xiang, Y.; Zhou, B.; Zhang, Y.; Wu, J.; Hu, R.; Liu, L.; Song, J.; Qu, J. Enhanced photocatalytic performance of Ag/TiO₂ nanohybrid sensitized by black phosphorus nanosheets in visible and near-infrared light. *J. Colloid Interface Sci.* **2019**, *534*, 1–11. [[CrossRef](#)] [[PubMed](#)]
120. Xu, Y.; Wang, X.; Jin, M.; Zhou, G.; Shui, L. Enhanced performance of dye-sensitized solar cells anodes modified with black phosphorus nanosheets. *J. Mater. Sci.* **2020**, *55*, 5499–5509. [[CrossRef](#)]
121. Song, J.; Wang, J.; Lin, X.; He, J.; Liu, H.; Lei, Y.; Chu, Z. Black Phosphorus/TiO₂ Composite Photoanode with Enhanced Photoelectrical Performance. *ChemElectroChem* **2017**, *4*, 2373–2377. [[CrossRef](#)]
122. Yin, X.; Tang, C.S.; Zheng, Y.; Gao, J.; Wu, J.; Zhang, H.; Chhowalla, M.; Chen, W.; Wee, A.T.S. Recent developments in 2D transition metal dichalcogenides: Phase transition and applications of the (quasi-)metallic phases. *Chem. Soc. Rev.* **2021**, *50*, 10087–10115. [[CrossRef](#)] [[PubMed](#)]
123. Chhowalla, M.; Liu, Z.; Zhang, H. Two-dimensional transition metal dichalcogenide (TMD) nanosheets. *Chem. Soc. Rev.* **2015**, *44*, 2584–2586. [[CrossRef](#)]
124. Choi, W.; Choudhary, N.; Han, G.H.; Park, J.; Akinwande, D.; Lee, Y.H. Recent development of two-dimensional transition metal dichalcogenides and their applications. *Mater. Today* **2017**, *20*, 116–130. [[CrossRef](#)]
125. Ali, M.; Afzal, A.M.; Iqbal, M.W.; Mumtaz, S.; Imran, M.; Ashraf, F.; Ur Rehman, A.; Muhammad, F. 2D-TMDs based electrode material for supercapacitor applications. *Int. J. Energy Res.* **2022**, *46*, 22336–22364. [[CrossRef](#)]
126. Rashidi, S.; Rashidi, S.; Heydari, R.K.; Esmaeili, S.; Tran, N.; Thangi, D.; Wei, W. WS₂ and MoS₂ counter electrode materials for dye-sensitized solar cells. *Prog. Photovolt. Res. Appl.* **2021**, *29*, 238–261. [[CrossRef](#)]
127. Gurulakshmi, M.; Meenakshamma, A.; Siddeswaramma, G.; Susmitha, K.; Venkata Subbaiah, Y.P.; Narayana, T.; Raghavender, M. Electrodeposited MoS₂ counter electrode for flexible dye sensitized solar cell module with ionic liquid assisted photoelectrode. *Sol. Energy* **2020**, *199*, 447–452. [[CrossRef](#)]
128. Vijaya, S.; Landi, G.; Wu, J.J.; Anandan, S. MoS₂ nanosheets based counter electrodes: An alternative for Pt-free dye-sensitized solar cells. *Electrochim. Acta* **2019**, *294*, 134–141. [[CrossRef](#)]
129. Krishnamoorthy, D.; Prakasam, A. Preparation of MoS₂/graphene nanocomposite-based photoanode for dye-sensitized solar cells (DSSCs). *Inorg. Chem. Commun.* **2020**, *118*, 108016. [[CrossRef](#)]
130. Menon, H.; Gopakumar, G.; Sankaranarayanan Nair, V.; Nair, S.V.; Shanmugam, M. 2D-Layered MoS₂-Incorporated TiO₂-Nanofiber- Based Dye-Sensitized Solar Cells. *ChemistrySelect* **2018**, *3*, 5801–5807. [[CrossRef](#)]
131. Xu, T.; Kong, D.; Tang, H.; Qin, X.; Li, X.; Gurung, A.; Kou, K.; Chen, L.; Qiao, Q.; Huang, W. Transparent MoS₂/PEDOT Composite Counter Electrodes for Bifacial Dye-Sensitized Solar Cells. *ACS Omega* **2020**, *5*, 8687–8696. [[CrossRef](#)]
132. Li, S.; Chen, Z.; Zhang, W. Dye-sensitized solar cells based on WS₂ counter electrodes. *Mater. Lett.* **2012**, *72*, 22–24. [[CrossRef](#)]
133. Krishnamoorthy, D.; Prakasam, A. Graphene Hybridized with Tungsten disulfide (WS₂) Based Heterojunctions Photoanode Materials for High Performance Dye Sensitized Solar Cell Device (DSSCs) Applications. *J. Clust. Sci.* **2021**, *32*, 621–630. [[CrossRef](#)]
134. Huang, J.; Qian, X.; Yang, J.; Niu, Y.; Xu, C.; Hou, L. Construction of Pt-free electrocatalysts based on hierarchical CoS₂/N-doped C@Co-WS₂ yolk-shell nano-polyhedrons for dye-sensitized solar cells. *Electrochim. Acta* **2020**, *340*, 135949. [[CrossRef](#)]
135. Hussain, S.; Patil, S.A.; Memon, A.A.; Vikraman, D.; Naqvi, B.A.; Jeong, S.H.; Kim, H.-S.; Kim, H.-S.; Jung, J. CuS/WS₂ and CuS/MoS₂ heterostructures for high performance counter electrodes in dye-sensitized solar cells. *Sol. Energy* **2018**, *171*, 122–129. [[CrossRef](#)]

Disclaimer/Publisher's Note: The statements, opinions and data contained in all publications are solely those of the individual author(s) and contributor(s) and not of MDPI and/or the editor(s). MDPI and/or the editor(s) disclaim responsibility for any injury to people or property resulting from any ideas, methods, instructions or products referred to in the content.